A major purpose of the Technical Information Center is to provide the broadest dissemination possible of information contained in DOE's Research and Development Reports to business, industry, the academic community, and federal, state and local governments.

Although a small portion of this report is not reproducible, it is being made available to expedite the availability of information on the research discussed herein.

1

LA-UR-83-3239

CONF-8310239--4

Los Alamos National Laboratory is operated by the University of California for the United States Department of Energy under contract W-7405-ENG-36.

LA-UR--83-3239

DE84 003777

TITLE: Particle and Field Signatures of Substorms in the Near Magnetotail

AUTHOR(S): D. N. Baker

SUBMITTED TO: Proceedings of Chapman Conference on Magnetic Reconnection, Los Alamos, NM, 3-7 October 1983

Los Alamos National Laboratory
Los Alamos, New Mexico 87545

Particle and Field Signatures of Substorms in the Near Magnetotail

D. N. Baker

Los Alamos National Laboratory, Los Alamos, NM 87545

Abstract The near-earth magnetotail ($10 \lesssim r \lesssim 20\ R_E$) portion of the terrestrial magnetosphere is very likely the region in which magnetospheric substorms are initiated and it is in this location that substorm-related magnetic reconnection appears to occur. An observational advantage compared to other astrophysical regions is that the near magnetotail can be nearly continuously monitored by spacecraft that are relatively fixed in location. Observations of magnetic fields and plasma distribution functions in the near-tail reveal a very regular and predictable sequence of variation in association with substorms. Following enhanced energy coupling between the solar wind and the magnetosphere, magnetic fields in the near-earth region exhibit a progressive development toward a more taillike configuration in the midnight sector. This taillike field is indicative of enhanced available free energy in the magnetotail which is eventually dissipated during substorms in episodes of magnetic reconnection. The development of a stressed, taillike magnetic field in the near-earth region leads to clear signatures in the distribution functions of energetic plasma particles wherein 10s of keV electrons exhibit a progressive transition away from a trapped distribution character ($j_\perp > j_\parallel$) to a field-aligned distribution character ($j_\parallel > j_\perp$). This effect can be readily understood in terms of azimuthal particle drifts in the distorted, taillike magnetic field and occurs for approximately 0.5-2.0 hours prior to substorm expansive phase onsets. Following substorm expansion onset (within a minute or so) there is a rapid relaxation of the stressed magnetic field configuration of the near-magnetotail around local midnight and there is invariably an associated injection of hot plasma and energetic particles into the region of geostationary orbit. These plasma populations appear to be directly related to the rapid conversion of stored magnetic energy at reconnection sites in a limited segment of the magnetotail plasma sheet. The higher energy (100s of keV) particle population appears to be accelerated very impulsively, probably due to intense induced electric fields in the magnetic merging region. These data, considered in a global context, provide very strong evidence for the neutral line substorm model and, thus, for the regular occurrence of magnetic reconnection in the near-earth magnetotail during substorms.

Introduction

Magnetic merging is thought to be an important form of energy conversion in a variety of cosmic settings including planetary magnetospheres and solar flare sites. The near-earth magnetotail portion of the terrestrial magnetosphere is very likely the region in which magnetospheric substorms are initiated and it is in this location that substorm-related magnetic reconnection appears to occur (Fig. 1).

Unlike many putative sites of reconnection which are totally inaccessible to direct in situ observation (e.g., the sun), or else are only occasionally sampled by fast-moving spacecraft (e.g., the magnetopause), the near magnetotail can be nearly continuously monitored by spacecraft that are relatively fixed in location. In particular, spacecraft at, or near, geostationary orbit remain approximately constant in radial distance and move slowly through the nightside region near the place where substorm reconnection normally begins.

Using observations from instrumentation aboard numerous geostationary satellites (Fig. 2) one can show that magnetic fields and plasma distribution functions undergo a very regular and predictable sequence of variation in association with substorms. Following enhanced coupling between the solar wind and the magnetosphere (associated with southward interplanetary field), magnetic fields in the near-earth region exhibit a progressive development toward a more taillike configuration in the midnight sector. This taillike field is indicative of enhanced cross-tail currents and, thus, of increased storage of magnetic energy in the tail lobes. This available free energy in the magnetotail is the energy which is eventually dissipated during substorms in episodes of magnetic reconnection.

The development of a stressed, taillike magnetic field in the vicinity of geostationary orbit (where the field configuration is ordinarily nearly dipolar) leads to clear signatures in the distribution functions of energetic plasma particles. In particular, it is regularly observed in association with taillike field development that 10s of keV electrons exhibit a progressive transition away from a trapped distribution character ($j_\perp > j_\parallel$) to a field-aligned distribution character ($j_\parallel > j_\perp$). This effect can be readily understood in terms of azimuthal particle drifts in the distorted, taillike magnetic field and occurs for approximately 0.5-2.0 hours prior to substorm expansive phase onsets.

Following substorm expansion onset (within a minute or so) there is a rapid relaxation of the stressed magnetic field configuration of the near-magnetotail around local midnight. Along with this dipolarization there is invariably the associated injection of hot plasma and energetic particles into the region of geostationary orbit. These plasma populations appear to be directly related to the rapid conversion of stored magnetic energy at reconnection sites in a limited segment of the magnetotail plasma sheet. The higher energy (100s of keV) particle population, further, appears to be accelerated very impulsively, probably due to intense induced electric fields in the magnetic merging region.

Once the substorm-generated hot plasma and energetic particle populations are injected into the inner magnetosphere, they tend to drift adiabatically in magnetically trapped orbits. The energetic particles, once produced, can provide a variety of tracer functions to determine characteristics of acceleration location and extent. These tracer aspects also include energy-dependent ion drift characteristics that allow identification of the principal region of overall substorm disturbance onset, ion gradient anisotropy information which allows the remote sensing of moving density-gradient boundaries in the vicinity of observing spacecraft, and, in a very recent discovery, charge-state-dependent ion drift characteristics that permit identification and discrimination between solar wind and ionospheric sources for the accelerated plasma which forms the energetic particle population (and eventually constitutes the terrestrial ring current).

In this paper we review many of the observations, and interpretations of such observations, which are supportive of the near-earth reconnection model of substorm energy dissipation.

Loading the Magnetospheric System

Numerous empirical studies of coupling between the solar wind and the magnetosphere (e.g., Nishida, 1983 and references therein) have shown the important role of the interplanetary magnetic field (IMF) orientation in determining the occurrence of geomagnetic (substorm) activity. When the IMF turns southward, strong substorm activity ordinarily follows after about one hour of persistently southward IMF. Figure 1, taken from a study by Baker et al. (1983a) for the Coordinated Data Analysis Workshop (CDAW) 6, shows the

relationship between a measure of solar wind energy input to the magnetosphere ($V \cdot B_z$) and substorm onset.

The solar wind speed (V) and IMF north-south component (B_z) observed at IMP-8 immediately upstream of the earth's magnetosphere showed a very clear example of a "southward turning" of B_z at 1010 UT on 22 March 1979. In Fig. 3 we plot $-V \cdot B_z$ (i.e., the east-west component of the interplanetary electric field) as an indicator of solar wind-magnetosphere coupling. Approximately 10 min after $-V \cdot B_z$ went positive we observed at 6.6 R_E that a very taillike magnetic field orientation began to occur. The field line inclination (0^o would be ~ dipolar, while 90^o would be ~ parallel to the ecliptic plane) measured at GOES-3 at geostationary orbit (~135^oW) is shown as the solid line. It is seen that between ~1025 UT and ~1055 UT the GOES-3 field line inclination reached $\gtrsim 60^o$ indicative of a very stressed, taillike field structure at 6.6 R_E. This is one of the classic signatures of the substorm growth phase (McPherron, 1970, 1972; Baker et al., 1978) and is the internal magnetosphere manifestation of the storage of energy in the near-earth magnetotail.

The expected effect of the kind of highly distorted, nondipolar magnetic field shown in Figure 3 would be to greatly distort trapped magnetospheric particle drift paths. Model calculations of azimuthal drift effects in a distorted magnetosphere are shown, for example, in Fig. 4 (Paulikas and Blake, 1979). As seen in this illustration, particles with equatorial pitch angles (α) near 0^o tend to drift nearer the earth at local noon and drift farther from the earth at local midnight. Conversely, $\alpha \approx 90^o$ particles drift very much closer to the earth at local midnight than at local noon. Since relatively strong inward radial gradients exist (higher flux for lesser geocentric radial distances) the effect of a distorted, taillike magnetic field structure near local midnight is to produce a local particle distribution with enhanced fluxes near $\alpha \approx 0^o$ and $\alpha \approx 180^o$ and a depletion of fluxes near $\alpha \approx 90^o$. Such "cigarlike" or "butterfly" bidirectional anisotropies are readily detected with present-day instrumentation.

An example of such effects is shown in Figure 5. Energetic electron data from two geostationary spacecraft 1977-007 and 1976-059, are shown for the period 0400-1000 UT on 8 September 1977. A substorm expansion onset occurred at 0720 UT on this day and this was observed at geostationary orbit as an "injection" of 30 to $\gtrsim$200 keV electrons. The injection of freshly accelerated

particles was seen both premidnight (S/C 1977-007) and postmidnight (S/C 1976-059).

As is particularly clear in the premidnight data in the upper panels of Fig. 5, an extended development of taillike magnetic field occurred at the 77-007 position. The field line inclination (θ_B) went from $\lesssim 20^\circ$ to $\sim 50^\circ$ between 0520 and 0720 UT. Accompanying this local field development, the energetic electron distributions became more and more cigarlike (as shown by the small inset panels of counts vs cosα). The parameter C_2 (Baker et al., 1978) is a measure of the amplitude and direction of the second-order electron anisotropy: $C_2 > 0$ indicates a field-aligned (cigar) distribution, while $C_2 < 0$ indicates a $j_\perp > j_\parallel$ (pancake) distribution. A strong and progressive development of cigarlike distributions occurred in the >30 keV electrons in accompaniment with the taillike stretching of the local magnetic field. A weak cigar phase was also seen, as indicated in Fig. 5, postmidnight at the 76-059 position.

Figure 6 shows the relationship of the C_2 parameter for 8 September (Fig. 5) to the concurrently measured IMF (sheath) orientation. As discussed by Baker et al. (1982b), it is observed that $\frac{dC_2}{dt}$ is positive for southward IMF ($\lambda_B < 0$), whereas $\frac{dC_2}{dt}$ is approximately 0 for northward IMF ($\lambda_B > 0$). Thus, southward IMF is clearly related to increased energy input to the magnetosphere which manifests itself as an increase of magnetotail currents and field strength, while northward IMF "turns off" energy input and rapidly stops the progress of energy storage in the tail field.

In studying hundreds of substorm events near local midnight with geostationary spacecraft instrumentation, we have found that most substorm injection events are preceded by cigar (growth) phase features of the type discussed above. Table 1 summarizes our findings concerning the occurrence of cigar phases prior to substorm expansion onsets. For more than 100 cases of detected cigar phases of 0.5 ~3.0 hour duration, in 97 cases the cigar phase was terminated by a substorm injection event. In only 4 cases did a cigar phase occur with no identifiable substorm onset. Conversely, when no cigar phase occurred when the geostationary spacecraft was in the nighttime sector we saw no substorms at all on 15 of those occasions and we saw some substorm activity on only 2 occasions. Table 1 is highly diagonal and suggests that substorm expansion onsets occur if, and only if, stored magnetotail energy is increased above a quiet time level.

Direct evidence is found in the more distant tail for the storage of magnetic energy as cigar phases develop near geostationary orbit. Figure 7 shows data from S/C 1976-059 at 6.6 R_E for portions of 28 and 29 December 1976. At 0100 UT a sharp, intense 800 nT negative magnetic bay occurred at ground stations near local midnight on 29 December 1976 (Baker et al., 1981) and intense substorm activity followed. The injection of energetic protons and electrons at 6.6 R_E at the substorm expansion onset (0100 UT) is well-illustrated in Figure 7 as is the very strong cigar phase evident in the lower panels of the figure. Between ~2330 UT and 0100 UT the field at geostationary orbit reached an inclination of nearly 90° ($\theta_B \sim 90°$) and C_2 became very large and positive ($C_2 \gtrsim 3.0$). This period, 2330-0100 UT, thus appears to have been an interval of strong magnetotail energy storage.

Concurrent data for this time from IMP-8 high in the southern tail lobe at ~35 R_E geocentric radial distance (and near local midnight) is shown in Figure 8. Ancillary data available (Baker et al., 1981) show that IMP-8 stayed near the magnetopause boundary for this entire interval and it is seen from the magnetic records of Figure 8 that $|\vec{B}|$ increased progressively from ~25 nT to ~40 nT between 2330 and 0100 UT. Thus, precisely during the geostationary orbit cigar phase, magnetotail energy densities greatly increased. Furthermore, right at the time of substorm expansion phase onset (and particle injections, Fig. 7) the magnetic energy density in the tail at ~35 R_E rapidly decreased (e.g., Fairfield and Ness, 1970). Figure 8 illustrates this feature very clearly since $|\vec{B}|$ decreased strongly and rapidly from 40 nT back to ~25 nT between 0100 and 0130 UT. Thus, the stored magnetic energy in the magnetotail was rapidly dissipated at substorm onset in this case.

Using ISEE-3 data in the very deep tail (80-220 R_E) we have now observed many examples of magnetotail diametrical expansion in association with cigar phases at 6.6 R_E. A typical example, shown in Figure 9, is that of 26 January 1983. ISEE-3 near the Y = 0 region of the aberrated tail at 220 R_E radial distance was located in the magnetosheath between 0800 and ~0910 UT. A cigar phase began at ~0850 at 6.6 R_E and culminated in a substorm expansion with sharp, dispersionless particle injection at 6.6 R_E at 0950 UT. At 1011 UT ISEE-3 instruments saw the plasma sheet suddenly envelop the spacecraft with plasma bulk flow velocities in excess of 1000 km/s at times (Hones et al., 1983).

The sequence of events in Fig. 9, borne out by many other examples (Baker et al., 1983b), is that energy storage near earth gives rise to the cigar phase signature. With ~20 minute delay, the distant (r ~220 R_E) tail increases substantially in diameter and ISEE-3 will then go progressively from the magnetosheath into the tail lobe. After a typical cigar phase development time (~1 hour) a substorm expansion phase onset with particle injection, etc., in the near-earth region occurs. Again, with a delay of 20-30 minutes from the time of near-tail onset phenomena, the hot, jetting plasmas of a reconnection-produced plasmoid (Hones et al., 1983) reach ISEE-3, having been released from the near-earth plasma sheet at substorm onset. We have seen many tens of these correlated events with near-midnight spacecraft at 6.6 R_E and ISEE-3 at 80-220 R_E. These results demonstrate quite clearly that the entire tail participates in the storage and sudden release of magnetic energy during substorms.

Unloading the Magnetospheric System

As the examples from the data presented above demonstrate, one cannot discuss the loading of the magnetosphere (growth phase) without discussing the expansive phase (unloading). These two parts of the substorm are intimately related and, indeed, during quite disturbed times the loading and unloading processes are often proceeding concurrently. As we strive to understand geomagnetic activity, however, it is normally very useful to begin by trying to comprehend simpler, less complicated events rather than immediately trying to untangle very complex, very disturbed geomagnetic patterns. As long as one recognizes that highly disturbed periods may represent a nonlinear superposition of effects seen during moderate substorm events, one often can get a clearer picture of substorm processes by examining details of relatively isolated events.

Figure 3 above demonstrated many of the gross temporal relationships that exist as one follows the flow of energy from the solar wind through the magnetosphere to its eventual dissipation in substorm processes. As noted previously, ~10 min after the southward turning of the IMF the growth phase of substorm activity began with taillike field development, etc. However, keeping with the general statistical results of Bargatze et al. (1983) and many other researchers (cf Nishida, 1983), the substorm expansion onset was delayed by a much longer time. In the case of 22 March 1979 shown in Fig. 3, the substorm

onset was very well identified to occur at ~1055 UT (McPherron and Manka, 1983). This initiation time is labelled "substorm onset" in Fig. 3 and is indicated by the vertical arrow. It followed the southward IMF turning by ~45 min.

Note that precisely at the substorm onset time in Fig. 3, the field inclination at 6.6 R_E went from $\theta_B \sim 65^o$ to $\theta_B \sim 20^o$. This rapid "dipolarization" is very characteristic of substorm expansion onsets and is generally seen in a region of several hours local-time width near midnight at geostationary orbit. (The second panel from the top of Fig. 5 and the second-to-bottom panel of Fig. 7 show precisely the same effect; cf. McPherron (1972) and Fairfield et al. (1981).) This dipolarization is taken as direct evidence for the diversion of a portion of the cross-magnetotail current through the ionosphere.

In general, observations show that a significant part of the energy stored in the magnetotail is dissipated through the ionospheric part of the so-called substorm current wedge. This substorm current wedge is set up by the sudden disruption of an azimuthally confined section of the enhanced cross-tail current and its diversion to the auroral ionosphere via field-aligned currents (cf. Fig. 10 and see McPherron et al. (1973) and Bostrom (1974)). The existence of the current wedge has been known for a long time from ground-based data and recent results have clarified the physical mechanism leading to its formation. Strong support for the neutral line model of substorms was obtained when three-dimensional MHD simulations of magnetotail reconnection (Birn and Hones, 1981, and Sato et al., 1983) showed that a pair of oppositely directed field-aligned currents are an inherent part of the neutral line model.

Geostationary satellites in the near-magnetotail show that the magnetospheric part of the substorm current wedge is azimuthally confined, has a geometry as shown in Fig. 10 and expands eastward and (especially) westward during the course of the substorm expansion phase (see Nagai, 1982 and Nagai et al., 1983). The near-earth part of the current wedge can also be studied by ground-based observations. Present results suggest that the substorm current wedge and the rapid dipolarization of magnetic fields near midnight at geostationary orbit are the direct results of the onset of magnetic reconnection in the near-tail region (10-20 R_E).

As demonstrated by the data of Figs. 5 and 7, the rapid collapse of the magnetic field at 6.6 R_E at substorm onset is accompanied in precise time coincidence by the sudden appearance of hot plasma (DeForest and McIlwain, 1971) and energetic particles. Note in Fig. 7, for example, that both electrons and ions up to >100 keV kinetic energy suddenly appear. The injection events become larger in flux amplitude as one goes to lower energy (Fig. 5, Fig. 7) and, in fact, the injection events are very prominent down into the plasma energy ($\lesssim$ 1 keV) regime (DeForest and McIlwain, 1971). Recall also from Fig. 8 that the appearance of these freshly injected particles occurs precisely during the time that magnetic energy density in the deep tail rapidly decreases. The evidence in many, many instances therefore points to a model in which stored magnetotail energy is rapidly converted to hot plasma and strong field-aligned currents which are resistively dissipated in the ionosphere.

Examination of the details of plasma and energetic particle properties during expansion phase onsets can reveal further important characteristics of such events. For example, it would be possible that particle flux variations at substorm onsets do not represent true flux variations, but rather are adiabatic changes associated with magnetic field increases and decreases. To test this, we have used combined plasma, energetic particle, and magnetic field data in another Coordinated Data Analysis Workshop (CDAW-2). Taking the phase space density as $f = j_\perp/2m_o\mu B$ (where m_o is the particle mass, μ is the magnetic moment of the particle, and B is the local field strength), we have calculated the variations of the distribution function of electrons and ions, at constant μ, for CDAW-2 time intervals (Baker et al., 1982a).

As is evident, the advantage of studying the phase space density at constant μ is that magnetic field variations are removed. Thus true particle density increases are revealed, and sources (or sinks) of particles can be identified.

The CDAW-2 analysis concentrated on a substorm onset which occurred at 1200 UT on 29 July 1977. Figure 11 shows examples of the phase space densities for electrons at μ = 1, 10, and 100 MeV/G. The most evident features in the upper panel (0300 UT (~1-300 keV in kinetic energy) grouping) were the following: (1) Even with removal of adiabatic effects, the flux dropout persists. (2) The phase space densities at constant μ were identical before the dropout (~1130 UT) and after the dropout (~1155 UT). (3) True phase space

density increases were observed for all magnetic moments (energies) after 1200 UT.

The points above, therefore, demonstrate that in a broad sector near local midnight there was a large-scale boundary motion that took the observing spacecraft into a low-density region (i.e., across a spatial discontinuity). This thinninglike event clearly preceded the substorm onset. Prior to the substorm onset the midnight sector spacecraft also returned to a predropout density configuration for several minutes (1155-1200 UT); this, therefore, clearly was not an injection event. At ~1200 UT an injection of newly accelerated or "fresh" particles occurred for all magnetic moments.

Thus, by examining geostationary orbit flux and phase space density variations (particularly near local midnight), it is established that fresh particles (up to several hundred MeV/G) appear at synchronous orbit during substorms. A remaining question about such particles is where the particles come from. The best available tool for examining the question of the general source region for the injected hot plasma and energetic particles is provided by ion gradient measurements. Because of their large gyroradii, 10-1000 keV ions can provide good information about density gradients that exist within a region of strong radial intensity variations or within an injected cloud of plasma and energetic particles [Fritz and Fahnenstiel, 1982; Walker et al., 1976].

The east-west gradient parameter is computed as follows:

$$A_{EW} = (E - W)/(E + W)$$

where E is the proton flux ($E_p > 145$ keV) measured in the sector with the detector looking eastward, and W is the proton flux measured looking westward. Given the direction of the normal magnetic field in the vicinity of the geostationary orbit satellites, and using the sense of gyration of protons, $A_{EW} > 0$ generally implies a higher density outside the spacecraft. For a stretched (taillike) magnetic field orientation (as distinguished from a completely dipolar field), one also obtains some secondary information from A_{EW}.

Figure 12 shows the A_{EW} (dashed line) values calculated for 29 July 1977 from the 77-007 energetic proton data (E > 145 keV). The solid line shows the measured >145 keV proton flux for the same interval. Looking at A_{EW} and intensity variations together, the following sequence of events is seen. Between 1155 and ~1200, i.e., during the recovery from the flux dropout, A_{EW} was strongly positive. This suggests that the higher particle density was inside the spacecraft. Since concurrent data showed the field to be very taillike during this period, the suggestion of a boundary motion during the dropout, with the high flux region moving earthward and equatorward, is fully borne out. As the fluxes recover, the spacecraft was enveloped from inside and from below.

At 1200 UT, A_{EW} went strongly negative. This period corresponded precisely to the first energetic particle and hot plasma injection into synchronous orbit. The character of A_{EW} showed that the injected particles came from outside the spacecraft location. The conclusion is therefore unambiguous in this case, viz., the injected particles arrive at 6.6 R_E from the outside and from above. This very likely means that these particles filled the high-latitude plasma sheet and that these filled field lines then collapsed inward over the spacecraft. After the leading edge of the particle injection passed over the spacecraft, A_{EW} went strongly positive (1202-1205 UT). This indicates that the highest particle density, after the injection, was generally inside 6.6 R_E.

From studies of the kind outlined above, there is little doubt that substorms produce freshly accelerated particles through the action of conversion of magnetic energy into particle kinetic energy. The data also suggest that this conversion generally occurs outside of geostationary orbit, deeper in the magnetotail plasma sheet.

Considerable progress has been made in understanding the acceleration and injection of hot plasma into the geostationary orbit region. For example, Moore et al. (1981) studied several substorms using data from ATS 6 and SCATHA (P78-2) with particular attention to the abrupt and dispersionless nature of the leading edges of many events. They found events which were abrupt at both spacecraft and travelled ~1 R_E in as little as one minute, implying average speeds up to 100 km/s and boundary thickness ~0.1 R_E. They further argued, on the basis of electron energy spectral changes that the moving plasma boundary which they referred to as the "injection front," was the precipitation-flow

boundary described by Kennel (1969). The plasma increases studied by Moore et al. (1981) were closely associated with large (factor 2-3) equally abrupt increases of local magnetic field strength and with rotations to a more dipolar orientation. On the basis of this fact, the agent of injection was identified as the earthward propagating compression wave previously observed by Russell and McPherron (1973). Such a compression wave will steepen and displace earthward any quiescent structures present in the plasma through which it propagates and thus qualitatively account for a sharp earthward moving boundary and for the displacement of plasma into regions where it would ordinarily be excluded.

These studies, while emphasizing the role of rapid boundary motion, have not indicated a total lack of local heating or acceleration. In fact, Moore et al. (1981) argued that multiple injections in a given evening had cumulative effects on the hot plasma being swept over the spacecrafts. Though the quasi-Maxwellian (multi-keV temperature) hot electron distribution was relatively unchanged in successive injections, a nonthermal power law tail of the distribution was enhanced at each injection. They speculated that an appreciable amount of each compression wave's energy was being dissipated in the inner plasma sheet.

It should be noted that the compression wave observed by Russell and McPherron (1973), and hypothesized as an agent of injection, contains a dawn-to-dusk directed current sheet and has an associated dawn-to-dusk directed induced electric field (~10 mV/m) which is consistent with recent electric field observations (Pedersen et al., 1978; Aggson et al., 1983). The motion of such a wave corresponds directly to the collapse of stretched magnetic field lines to a less stretched configuration (cf. Baker et al., 1982a), the collapse being communicated to more earthward locations by the propagating wave. An interesting aspect of such a wave is that it propagates into a region of decreasing phase speed. This is due to the increase in plasma density and decrease in ion mean energy associated with the plasmasphere, which is often appreciable near synchronous orbit. In such circumstances, the wave will steepen and may break, forming a shock, or be reflected. In either case, it should be unable to propagate very deeply into the plasmasphere, and there should be a well defined earthward limit of injection effects.

The compression wave hypothesis addresses the transport of tail plasmas, but it does not explain the dispersional features that are observed. Both transport and dispersion may be accommodated by bringing together the compression wave model and the injection boundary model (Mauk and McIlwain, 1974). This can be accomplished by hypothesizing that the propagating plasma sheet inner edge (injection front) has an earthward displacement which maximizes in the midnight sector. This earthward displacement may or may not correspond to the earthward-most propagation of the compression wave. The key to the validity of this combined model would be a demonstration that the near-midnight bulge configuration, required of the injection boundary, results from the compression wave displacement in a natural way. A schematic illustration of the required behavior is shown in Figure 13.

One consequence of the injection processes described above is contribution to the formation of the ring current distributions. The ring current particles reside in the inner magnetospheric regions (r ~2-6 R_E) and they give rise to depression in low latitude ground magnetic measurements (characterized by the Dst index). Evidence has been given that directly driven, non-impulsive, processes contribute to the formation of the ring current and such contributions are likely to take the form of enhanced global convection (Harel et al., 1981). However, as discussed earlier, the particle features observed in the geosynchronous regions are not consistent with global convective transport of particles from the outer magnetospheric region. Impulsive injection with characteristics distinct from global convection appear to dominate the earthward transport of particle near the geosynchronous orbit. These impulsively transported particles must play a role in the ring current formation, but the relative importance of the impulsive and driven processes remains to be determined. One role that the driven or convective processes may play is to transport further earthward the particles which have been impulsively transported to the geosynchronous regions (e.g., Lyons and Williams, 1980).

The energization mechanisms described above do not appear capable of producing the high energy (>100 keV) component of substorm-related particle enhancements. Such particles could, however, be rapidly accelerated in the parallel electric field which exists along a near-earth neutral line. Note that induction effects related to dynamic reconnection can raise the total potential drop along the neutral line far above its expected steady-state value

(Baker et al., 1982a). Moreover, acceleration processes at the neutral line could explain the electron heating pulse observed during some reconnection events (Bieber et al., 1982). Such heating is reminiscent of the laboratory reconnection results of Stenzel et al. (1982).

As has been shown above, enhancements of the fluxes of particles having energies of several hundred keV are commonly observed at synchronous orbit and in the magnetotail during geomagnetically active periods. In nearly all cases these flux enhancements are closely associated with individual magnetospheric substorms. As we have demonstrated here using energetic particle data from synchronous orbiting satellites and from satellites in the magnetotail, it is found that many features of the timing of particle enhancements relative to substorm onsets and recoveries (derived from ground magnetic records) and relative to plasma sheet thinnings and recoveries (measured with plasma probes on earth-orbiting satellites) can be understood in terms of the neutral line model of substorms in which the particles are impulsively accelerated during a brief period at substorm onset near a site of magnetic reconnection.

Particularly striking are very high energy proton (ion) phenomena associated with substorms. In approximately 10-20% of substorms, >0.3 MeV ions appear throughout the magnetosphere and its environs in close association with expansion phase onset (Belian et al., 1978). Oftentimes, ion bursts may be identifiable as distinct particle bunches ("drift echoes") which drift azimuthally around the earth through several (as many as 5) circulations (cf. Fig. 14). A comprehensive model for the morphology of energetic ion enhancements is illustrated in Figure 15 (Baker et al., 1979). This model suggests that after acceleration at the substorm X-line in the plasma sheet, the ions stream both sunward and tailward. Those reaching the synchronous orbit region are transported westward around the earth via curvature and grad-B drifts.

The tailward-streaming ions produced at the same time as drift-echo ions appear as "impulsive bursts". The inverse velocity dispersion (i.e., observation of slower particles before faster ones) exhibited by these bursts is supportive of their hypothesized origin at a magnetic X-line (Sarris and Axford, 1979). As suggested by the inset at the bottom of Figure 15, a spacecraft in the thinning plasma sheet successively samples field lines that have reconnected more and more recently at the X-line. These field lines contain ion distributions that are less depleted at the high energy end of the

spectrum by escape of the faster particles. Finally, just as the spacecraft enters the lobe, it samples preferentially the fastest ions streaming along field lines connected directly to the X-line source. Concurrent plasma observations confirm that impulsive bursts do indeed occur right at times of plasma dropouts (Belian et al., 1981).

As a final component of this picture, the more commonly observed non-impulsive (rapid-rise, slow-decay) plasma sheet ion enhancements are attributed in this model to envelopment of the observing satellite by the recovering (i.e., expanding) plasma sheet, into which have leaked ions previously injected into the outer radiation zone. The subsequent decay is explained by a combination of plasma sheet expansion, adiabatic cooling, and escape mechanisms. Escape from the magnetotail could in turn account for the appearance of energetic proton bursts in the magnetosheath and upstream region.

Although the number densities of energetic particles are relatively small compared to plasma number densities, the energy density in this component can be reasonably large throughout the outer trapping region and the magnetotail. Furthermore, once such particles are produced, they make excellent diagnostic tools for establishing substorm timing (e.g., Belian et al., 1981), for examining field line topology, and for remotely probing plasma boundary motions (e.g., Baker et al., 1982a).

An interesting application of the observation of drift-echo ion events comes about from the close inspection of the temporal and compositional characteristics of such events. Drift echo peaks frequently are observed to have a complex shape and do not always exhibit a simple rise and fall. One sees several peaks very close together. These "structured peaks" could result from several causes including: an injection multiple in time or longitude; there being more than one relatively abundant charge state of a given ion; multiple ion species being detected in a single sensor; and charge exchange causing the charge state of an individual ion to vary significantly on the drift time scale. Observation of the evolution of a structured peak with longitudinal drift can help to distinguish between some of these possibilities.

The angular velocity Ω_3 associated with the azimuthal drift of an energetic ion is given by the relationship (cf., Blake et al., 1983)

$$\Omega_3 = f(\alpha_0)IE/q$$

where E is the kinetic energy of the ion, q is the charge state and α_o the equatorial pitch angle. Here it is assumed (as is the case for drift-echo events) that the energy of the ion is sufficiently high ($E \gtrsim 100$ keV) that the effect of magnetospheric electric fields on drift is not significant. The important feature to note for present purposes is that the drift velocity of an ion at a given L value and pitch angle depends upon the ratio of its energy to the effective charge of the ion. Thus a measurement of the drift speed and the energy of an ion determines the charge state.

The mean charge states of heavy ions trapped in the earth's magneotsphere, in particular those of the abundant heavy ions He, C, and O, are important obervational parameters predicted by various theories (e.g., Spjeldvik and Fritz, 1978) of the origin and evolution of the magnetospheric plasma. Up to the present time satellite instrumentation capable of determining the charge state of heavy ions with energies above ~50 keV has not been flown. Consequently there is motivation to develop indirect methods of determining the charge state of energetic magnetospheric ions, even if such methods do not have universal applicability. One such method is to measure the drift speed of an ion in the magnetic field of the earth.

A major difficulty is to tag an ion in some way in order to be able to measure its drift speed. The experimental procedure employed by Blake et al. (1983) utilizes observations of the transient, highly peaked enhancements in the ion fluxes represented by ion drift echo events. An ion drift echo event seen in several proton channels and two helium channels onboard the SCATHA spacecraft between 2100 and 2200 UT on 25 February 1979 is shown in Figure 16.

The countrates as a function of time in Figure 16 are for pitch angles of 90° ±30°. The drift speed of an ion is a function of pitch angle, but a dipolar calculation predicts only a 5% difference between the extremes of 60° and 90°. The dispersion in arrival time as a function of ion energy can be seen clearly in Figure 16 although, because of the averaging of the data that was done to generate the figure, it cannot be used for quantitative timing purposes. Note that the peak in the 363-717 keV proton channel occurs prior to either of the helium peaks. In other data (Blake et al., 1983) not shown here it was seen that there was only one CNO count in the five hours preceding the event, and it was in the lowest energy channel; the observed CNO counts could, therefore, also be associated with the drift echo event with confidence.

The results of the Blake et al. study show that the helium ions were fully stripped (charge state +2), and that the CNO ions observed by SCATHA were probably of charge state 5 or higher, and definitely not charge state 1 or 2. These results indicate that the source of the accelerated plasma was not the ionosphere. Furthermore the plasma could not have been resident in the synchronous altitude region for a long time before acceleration. If it had been, then charge exchange would have transformed the stripped, or nearly stripped, solar wind ions (Spjeldvik and Fritz, 1978) to a lower charge state than observed. A model in which plasma sheet ions, originally from the solar wind, are brought in from the tail and accelerated would fit the observations.

As discussed by Blake et al. (1983), studies have shown that the energetic heavy-ion fluxes in the synchronous altitude region are highly time variable and that, above a few hundred keV, CNO ions are the most abundant. These results suggest that the most-energetic ions in the synchronous altitude region result from injections of plasma sheet ions accelerated by strong electric fields. If the plasma had a steep energy spectrum prior to acceleration, the several-fold increase in the CNO energy relative to that of protons, because of their high charge state, could make them most abundant in the energized plasma population.

Summary

Observations in the near-earth magnetotail show some of the clearest and most repeatable signatures available in support of the concept of loading and unloading of magnetic energy in association with substorms. The data illustrate that magnetic energy is accumulated and stored for 0.5 ~2.0 hours in the tail lobes and then is rapidly dissipated at substorm expansion onset. The dissipation is manifested by the acceleration and rapid transport of hot plasma and energetic particle populations within the near-tail region. These energized plasmas provide an excellent tracer capability which allows a relatively clear determination of where, when, and how magnetic energy is converted to other forms during substorms.

When near-tail data are considered in a global context of deep-tail measurements, numerical models, ground-based data, etc., they provide very strong evidence for the neutral line substorm model and, thus, for the regular occurrence of magnetic reconnection in the near-earth magnetotail.

Acknowledgments

The author would like to thank the many colleagues who have contributed significantly to the work reviewed in this paper. In particular, thanks are extended to E. Hones, R. Belian, P. Higbie, T. Fritz, J. Gosling, S. Bame, and R. Zwickl of Los Alamos, R. McPherron of UCLA, and J. Blake and J. Fennell of Aerospace Corporation. Sincere appreciation is also extended to M. Halbig, R. Robinson, E. Tech, and R. Anderson for data analysis support. Very useful discussions with K. Schindler and A. Nishida are gratefully acknowledged.

REFERENCES

Aggson, T. L., J. P. Heppner, and N. C. Maynard, Observations of large magnetospheric electric fields during the onset phase of a substorm, J. Geophys. Res., 88, 3981, 1983.

Baker, D. N., P. R. Higbie, E. W. Hones, Jr., and R. D. Belian, High-resoluton energetic particle measurements at 6.6 R_e, 3, Low-energy electron anisotropies and short-term substorm predictions, J. Geophys. Res., 83, 4863, 1978.

Baker, D. N., R. D. Belian, P. R. Higbie, and E. W. Hones, Jr., High-energy magnetospheric protons and their dependence on geomagnetic and interplanetary conditions, J. Geophys. Res., 84, 7183, 1979.

Baker, D. N., E. W. Hones, Jr., P. R. Higbie, R. D. Belian, and P. Stauning, Global properties of the magnetosphere during a substorm growth phase: A case study, J. Geophys. Res., 86, 8941, 1981.

Baker, D. N., T. A. Fritz, B. Wilken, P. R. Higbie, S. M. Kaye, M. G. Kivelson, T. E. Moore, W. Studemann, A. J. Masley, P. H. Smith, and A. L. Vampola, Observation and modeling of energetic particles at synchronous orbit on July 29, 1977, J. Geophys. Res., 87, 5917, 1982a.

Baker, D. N., E. W. Hones, Jr., R. D. Belian, P. R. Higbie, R. P. Lepping, and P. Stauning, Multiple-spacecraft and correlated riometer study of magnetospheric substorm phenomena, J. Geophys. Res., 87, 6121, 1982b.

Baker, D. N., et al., Evidence for magnetotail energy storage and sudden release during substorms of the CDAW-6 intervals, J. Geophys. Res., to be submitted, 1983a.

Baker, D. N., S. J. Bame, R. D. Belian, W. C. Feldman, J. T. Gosling, P. R. Higbie, E. W. Hones, Jr., D. J. McComas, and R. D. Zwickl, Correlated dynamical changes in the near-earth and distant magnetotail regions: ISEE-3, J. Geophys. Res., submitted, 1983b.

Bargatze, L. F., D. N. Baker, R. L. McPherron, and E. W. Hones, Jr., Magnetospheric response for many levels of geomagnetic activity, J. Geophys. Res., in press, 1983.

Belian, R. D., D. N. Baker, P. R. Higbie, and E. W. Hones, Jr., High-resolution energetic particle measurements at 6.6 R_E, 2, High-energy proton drift echoes, J. Geophys. Res., 83, 4857, 1978.

Belian, R. D., D. N. Baker, E. W. Hones, Jr., P. R. Higbie, S. J. Bame, and J. R. Asbridge, Timing of energetic proton enhancements relative to magnetospheric substorm activity and its implication for substorm theories, J. Geophys. Res., 86, 1415, 1981.

Bieber, J. W., E. C. Stone, E. W. Hones, Jr., D. N. Baker, and S. J. Bame, Plasma behavior during energetic electron streaming events: further evidence for substorm-associated magnetic reconnection, Geophys. Res. Lett., 9, 664, 1982.

Birn, J. and E. W. Hones, Jr., Three-dimensional computer modeling of dynamic reconnection in the geomagnetic tail, J. Geophys. Res., 86, 6802, 1981.

Blake, J. B., J. F. Fennell, D. N. Baker, R. D. Belian, and P. R. Higbie, A determination of the charge state of energetic magnetospheric ions by the observation of drift echoes, Geophys. Res. Letters, in press, 1983.

Bostrom, R., Ionosphere-magnetosphere coupling, in: Magnetospheric Physics, B. M. McCormac (ed.), pp. 45-59, Dordrecht, D. Reidel, 1974.

DeForest, S. E., and C. E. McIlwain, Plasma clouds in the magnetosphere, J. Geophys. Res., 76, 3587, 1971.

Fairfield, D. H., and N. F. Ness, Configuration of the geomagnetic tail during substorms, J. Geophys. Res., 75, 7032, 1970.

Fairfield, D. H., R. P. Lepping, E. W. Hones, Jr., S. J. Bame, and J. R. Asbridge, Simultaneous measurements of magnetotail dynamics by IMP spacecraft, J. Geophys. Res., 86, 1396, 1981.

Fritz, T. A., and S. C. Fahnenstiel, High temporal resolution energetic particle soundings at the magnetopause on November 8, 1977, using ISEE-2, J. Geophys. Res., 87, 2125, 1982.

Harel, M., R. A. Wolf, R. W. Spiro, P. H. Reiff, C.-K. Chen, W. J. Burke, F. J. Rich, and M. Smiddy, Quantitative simulation of a magnetospheric substorm, 2. Comparison with observations, J. Geophys. Res., 86, 2242, 1981.

Hones, E. W., Jr., D. N. Baker, S. J. Bame, W. C. Feldman, J. T. Gosling, D. J. McComas, R. D. Zwickl, J. Slavin, E. J. Smith, B. T. Tsurutani, Structure of the magnetotail at 220 R_E and its response to geomagnetic activity, Geophys. Res. Letters, submitted, 1983.

Kennel, C. F., Consequences of a magnetospheric plasma, Rev. Geophys. Sp. Phys., 7, 379, 1969.

Lyons, L. R., and D. J. Williams, A source for the geomagnetic storm main phase ring current, J. Geophys. Res., 85, 523, 1980.

Mauk, B. H., and C. E. McIlwain, Correlation of Kp with the substorm-injected plasma boundary, J. Geophys. Res., 79, 3193, 1974.

McPherron, R. L., Growth phase of magnetospheric substorms, J. Geophys. Res., 28, 5592, 1970.

McPherron, R. L., Substorm related changes in the geomagnetic tail: The growth phase, Planet. Space Sci., 20, 1521, 1972.

McPherron, R. L., and P. H. Manka, Dynamics of the March 22, 1979 substorm event: CDAW-6, J. Geophys. Res., in preparation, 1983.

McPherron, R. L., C. T. Russell, and M. P. Aubry, Satellite studies of magnetospheric substorms on August 15, 1968, 9. Phenomenological model for substorms, J. Geophys. Res., 78, 3131, 1973.

Moore, T. E., R. L. Arnoldy, J. Feynman, and D. A. Hardy, Propagating substorm injection fronts, J. Geophys. Res., 86, 6713, 1981.

Nagai, T., Local-time dependence of electron flux changes during substorms derived from multi-satellite observation at synchronous orbit, J. Geophys. Res., 87, 3456, 1982.

Nagai, T., D. N. Baker, and P. R. Higbie, Development of substorm activity in multiple onset substorms at synchronous orbit, J. Geophys. Res., in press, 1983.

Nishida, A., IMF control of the earth's magnetosphere, Space Sci. Rev., 34, 185, 1983.

Paulikas, G. A., and J. B. Blake, Effects of the solar wind on magnetospheric dynamics: energetic electrons at the synchronous orbit, in Quantitative Modeling of Magnetospheric Processes, W. P. Olson (Editor), American Geophys. Union, Washington, D.C., 1979.

Pedersen, A., R. Grard, K. Knott, D. Jones, and A. Goufalone, Measurements of quasi-static electric fields between 3 and 7 earth radii on Geos-1, Space Sci. Rev., 22, 333, 1978.

Russell, C. T. and R. L. McPherron, The magnetotail and substorms, Space Sci. Rev., 15, 205, 1973.

Sarris, E. T. and W. I. Axford, Energetic protons near the plasma sheet boundary, Nature, 77, 460, 1979.

Sato, T., T. Hayashi, R. J. Walker, and M. Ashour-Abdalla, Neutral sheet current interruption and field-aligned current generation by three dimensional driven reconnection, Geophys. Res. Letters, 10, 221, 1983.

Spjeldvik, W. N., and T. A. Fritz, Theory for charge states of energetic oxygen ions in the earth's radiation belts, J. Geophys. Res., 83, 1583, 1978.

Stenzel, R. L., W. Gekelman, and N. Wild, Magnetic field line reconnection experiments, 4. Resistivity, heating, and energy flow, J. Geophys. Res., 87, 111, 1982.

Walker, R. J., K. N. Erickson, R. L. Swanson, and J. R. Winckler, Substorm-associated particle boundary motion at synchronous orbit, J. Geophys. Res., 81, 5541, 1976.

Figure Captions

Fig. 1. A model depicting the sequence of events occurring in a magnetospheric substorm.

Fig. 2. A typical constellation of spacecraft that is available at (or near) geostationary orbit for the study of substorm effects in the near-tail region.

Fig. 3. A comparison of a solar wind energy input function ($-VB_z$, dashed line) as compared with the GOES-3 magnetic field line inclination (θ_B, solid line) measured at synchronous orbit for a portion of 22 March 1979. As discussed in the text, a substorm growth phase was observed for ~1/2 hour prior to substorm expansion onset (at ~1055 UT) and this growth phase was manifested by an extreme taillike field development near local midnight at geostationary orbit (from Baker et al., 1983a).

Fig. 4. Representative electron drift paths (equatorial crossing altitudes) for those particles mirroring near the equator (EPA = 90^o) and those mirroring at high latitudes (EPA = 0^o) (from Paulikas and Blake, 1979).

Fig. 5. A detailed plot of the geostationary orbit spin-averaged energetic electron fluxes, local magnetic field line tilt angle (θ_B), and second-order anisotropy amplitude (C_2) on September 8, 1977. All electron channels (energies as labeled) have a common upper cutoff energy of 300 keV. The upper panels show data for spacecraft 1977-007, while the lower panels show data for spacecraft 1976-059. Universal time is shown along the bottom of the figure, while geographical local time is shown for each satellite. A substorm injection event is seen at ~0720 UT, preceded by a substorm growth (cigar) phase of ~2-hour duration. (From Baker et al., 1982b)

Fig. 6. A detailed comparison of the concurrently measured magnetic field inclination (λ_B) at EMT 8 and the second-order electron anisotropy amplitude (C_2) at spacecraft 1977-007. The figure shows data for

September 8, 1977 (compare Fig. 5). Periods of southward sheath or interplanetary fields ($\lambda_B < 0$) have been emphasized by black shading, while times of strong northward or southward rotation of λ_B are shown by the vertical dashed lines. Periods of positive growth of C_2 are seen to correspond to $\lambda_B < 0$, while periods of constant C_2 correspond to $\lambda_B > 0$. (From Baker et al., 1982b)

Fig. 7. A plot similar to Fig. 5 showing electron and proton differential fluxes as labelled for a portion of 28 and 29 December 1976. As described in the text, a substorm growth phase was observed from ~2330 to 0100 UT at which time a substorm expansion phase commenced (from Baker et al., 1981).

Fig. 8. IMP 8 magnetic field data showing 15.36-s field averages from 1800 UT on December 28 to 0300 UT on December 29, 1976. The upper panel shows the total field B, while the succeeding lower panels show the X, Y, and Z vector components of B in solar magnetospheric coordinates. IMP 8 was located in the high southern tail region at this time at ~ local midnight. At 1800 UT the GSM coordiates (in R_E) were X = -30.7, Y = 0.1, Z = -16.8, while at 0300 UT the spacecraft coordinates were X = -32.5, Y = -5.9, Z = -13.9. (From Baker et al., 1981).

Fig. 9. A comparison of ISEE-3 electron distribution function moments at ~220 R_E in the center of the distant magnetotail with measurements from spacecraft 1981-025 at geostationary orbit (~135°W) near local midnight. The substorm growth, or cigar, phase at 6.6 R_E occurred as indicated between ~0850 UT and ~0950 UT at which time a sharp, intense substorm expansion phase onset occurred. With delays of 20-30 minutes, ISEE-3 saw closely related events such that at ~0910 UT it went from the sheath into the tail lobe and at ~1011 UT it went from the lobe into the plasma sheet where very high tailward plasma flows were seen. These data show that the very distant tail expands during growth phases as energy is added to the tail lobes (from Baker et al., 1983b).

Fig. 10. Schematic drawing of current flow on the nightside of the inner magnetosphere during a substorm. Current flowing across the tail has been diverted into the ionosphere along field lines to form the substorm electrojet (From McPherron et al., 1973).

Fig. 11. Electron phase space density variations (computed as described in the text) for the 1200 UT substorm period on 29 July 1977. Densities at constant first invariant values (μ, as labeled) are plotted (from Baker et al., 1982a).

Fig. 12. A comparison of the >145-keV proton flux (solid line) and the associated east-west gradient anisotropy (dotted line) for the period illustrated in Fig. 11. Strong gradient anisotropies occur as new energetic particles are injected near synchronous orbit (from Baker et al., 1982a).

Fig. 13. Equatorial plane schematic of an hypothesis concerning the formation of an injection boundary near synchronous orbit. A compression wave impulse propagates earthward from the magnetotail through the pre-existing inner edge of the plasma sheet, producing an earthward moving injection front with maximum net displacement in a sector near midnight (from T. E. Moore and B. H. Mauk, private communication, 1983).

Fig. 14. The upper panel is a representative illustration of an energetic ion drift echo event as observed by spacecraft 1976-059 on 14 April 1977. Two energy channels are shown (0.4-0.5 MeV and 0.5-0.6 MeV) and the left-hand inset illustrates that the first of the 5 drift echoes seen occurred at precisely the time of a substorm expansion onset seen at Leirvogur, Iceland. The middle panel is for a similar event on 30 July 1976 and shows a plot of azimuthal position of occurrence of proton drift echo pulses versus the UT of their observation at the spacecraft. Several energy ranges, as labeled, are included in the analysis, and the intersection of the several lines indicates the time and location of the proton injection. The lower panel shows the Guam

magnetogram for 1100-1400 UT of July 30, 1976 and shows a substorm expansion onset at precisely 1237 UT (from Belian et al., 1978, 1981).

Fig. 15. Schematic depicting the sequence of energetic particle events predicted by the model of Baker et al. (1979). (a) The inner magnetosphere just prior to substorm onset showing the buildup of stress evidenced by the taillike field. (b) The magnetosphere just after onset showing a dipolar field configuration and the accelerated ion bunches streaming sunward toward the trapped radiation zones and antisunward along the thinning plasma sheet. (c) Conditions just prior to substorm recovery and the beginning of the plasma sheet expansion. (d) Expansion of the plasma sheet and the subsequent filling of the expanding sheet with energetic protons diffusing out of the trapped region.

Fig. 16. The temporal history of proton and helium ion count rates for a drift echo event measured by SCATHA instruments on 25 February 1979. As described in the text, examination of the relative timing of H and He peaks allows a charge state determination of the heavier ions (from Blake et al., 1983).

Table 1.

PRECURSORY CIGAR-PHASE ASSOCIATION WITH SUBSTORMS

	NO SUBSTORM	SUBSTORM OBSERVED
NO CIGAR-PHASE OBSERVED	15	2
CIGAR-PHASE OBSERVED	4	97

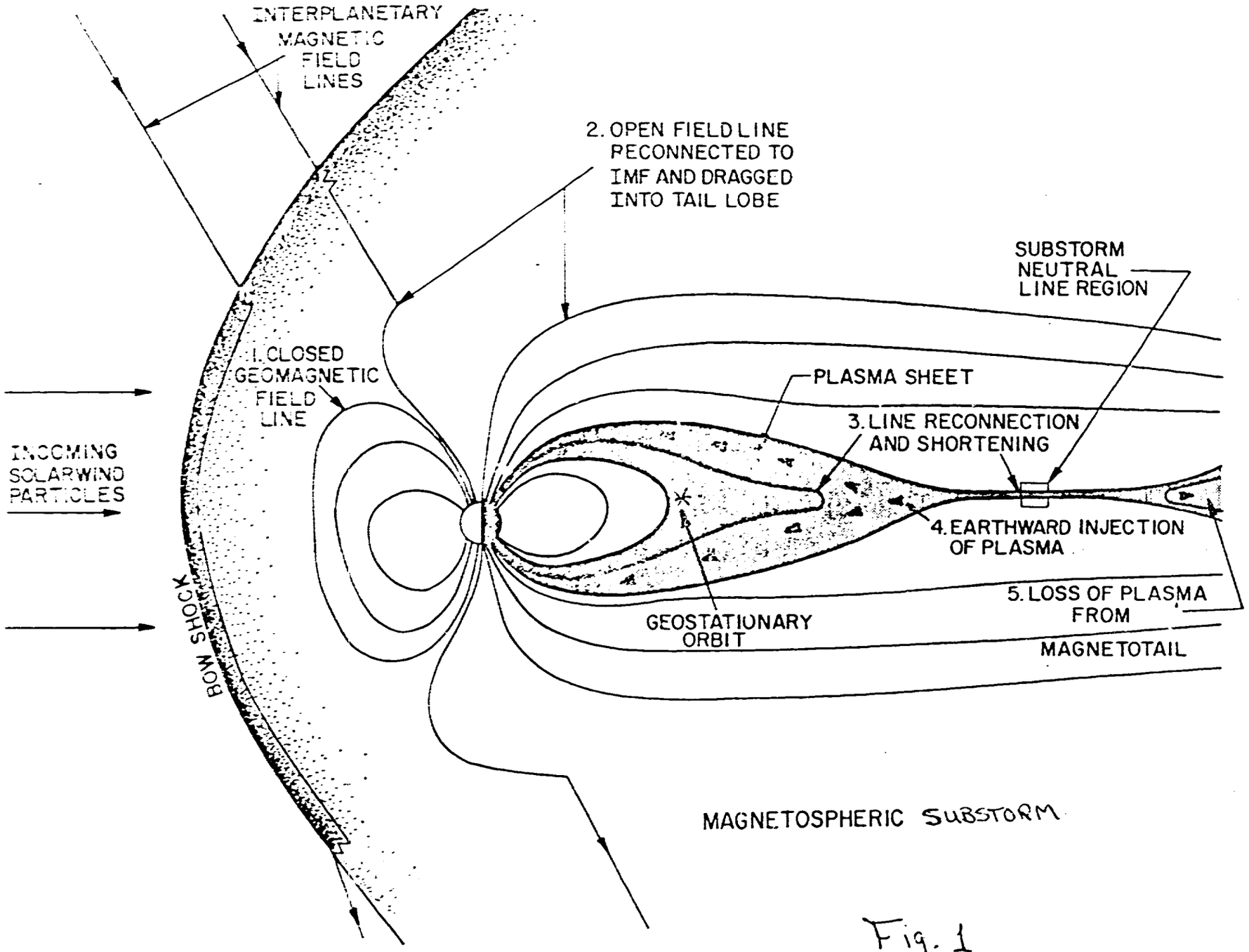
INTERPLANETARY
MAGNETIC
FIELD
LINES
2. OPEN FIELD LINE
RECONNECTED TO
IMF AND DRAGGED
INTO TAIL LOBE
SUBSTORM
NEUTRAL
LINE REGION
1. CLOSED
GEOMAGNETIC
FIELD
LINE
PLASMA SHEET
3. LINE RECONNECTION
AND SHORTENING
INCOMING
SOLARWIND
PARTICLES
4. EARTHWARD INJECTION
OF PLASMA
BOW SHOCK
5. LOSS OF PLASMA
FROM
MAGNETOTAIL
GEOSTATIONARY
ORBIT
MAGNETOSPHERIC SUBSTORM

Fig. 1

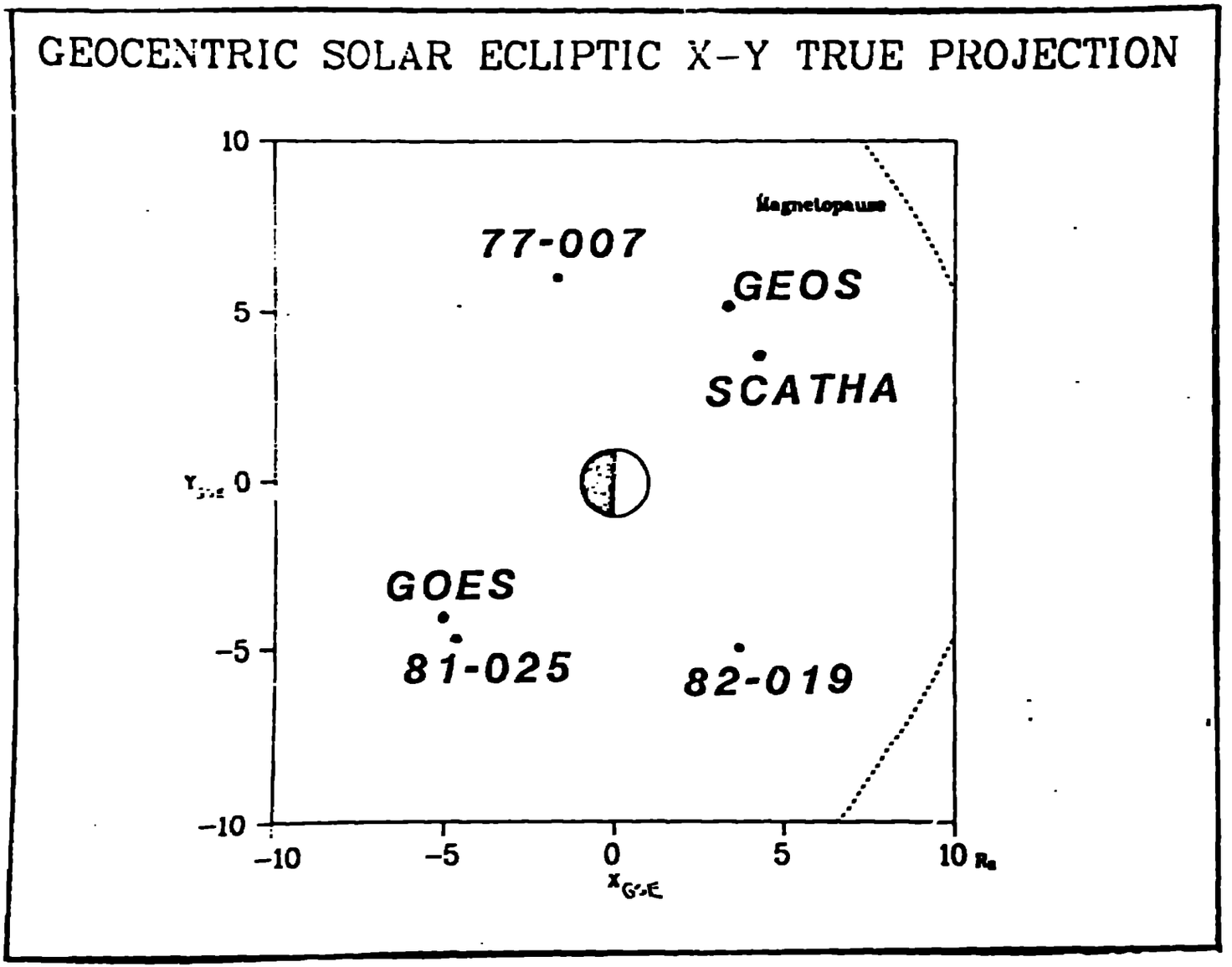
GEOCENTRIC SOLAR ECLIPTIC X–Y TRUE PROJECTION
10
5
0
−5
−10
−10
−5
0
5
10 R
Magnetopause
77-007
GEOS
SCATHA
GOES
81-025
82-019

Fig. 2

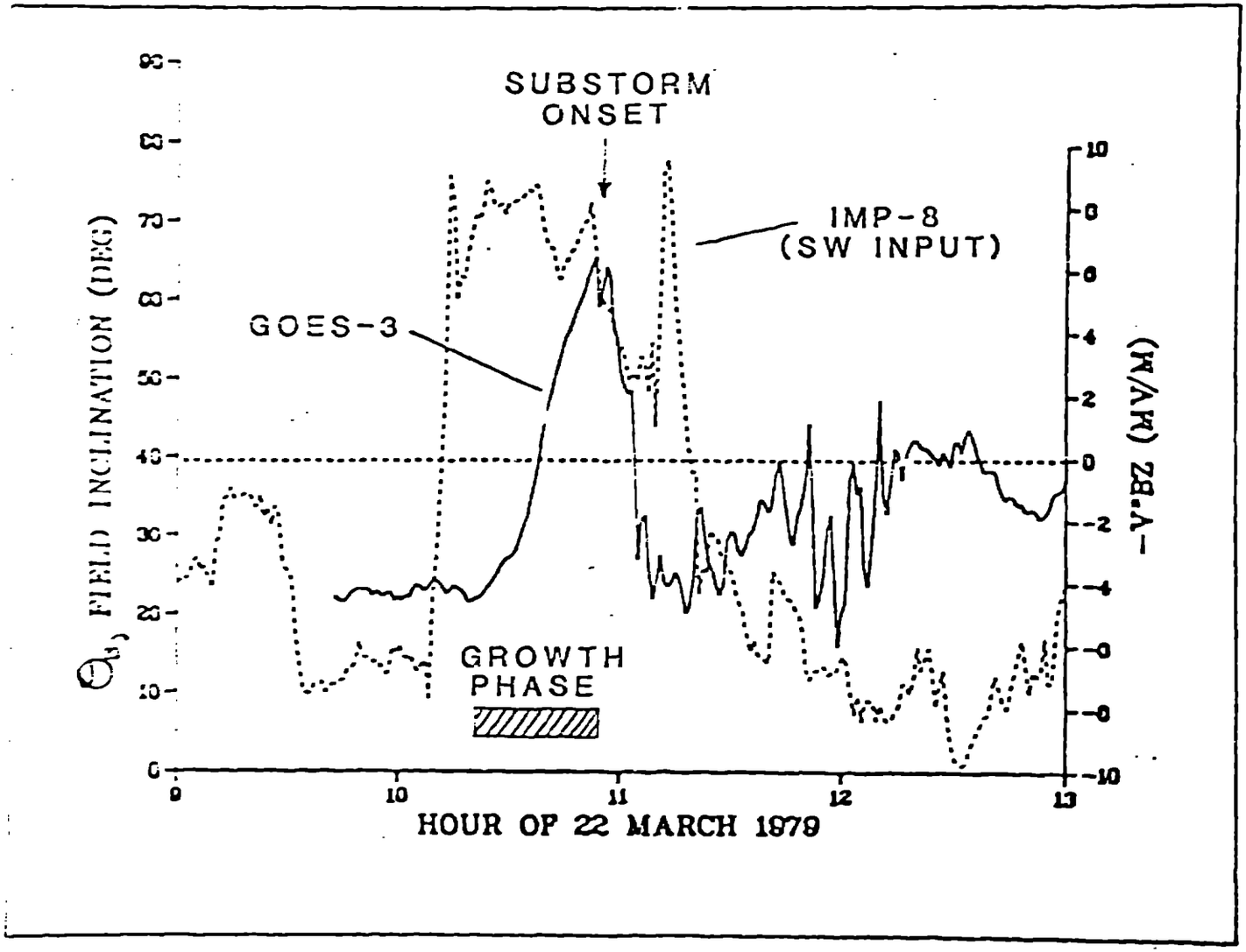
SUBSTORM
ONSET
IMP-8
(SW INPUT)
GOES-3
GROWTH
PHASE
Θ_B FIELD INCLINATION (DEG)
$-V_x B_z$ (MV/M)
HOUR OF 22 MARCH 1979

Fig 3

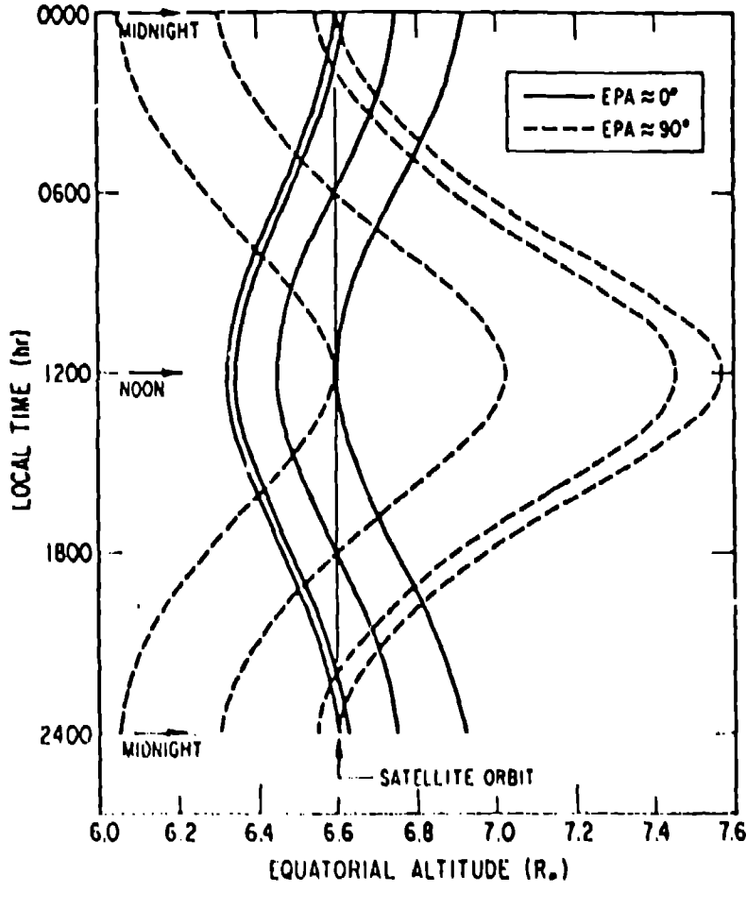
0000
MIDNIGHT
0600
1200
NOON
1800
2400
MIDNIGHT
LOCAL TIME (hr)
EPA ≈ 0°
EPA ≈ 90°
SATELLITE ORBIT
6.0
6.2
6.4
6.6
6.8
7.0
7.2
7.4
7.6
EQUATORIAL ALTITUDE (R.)

Fig 1

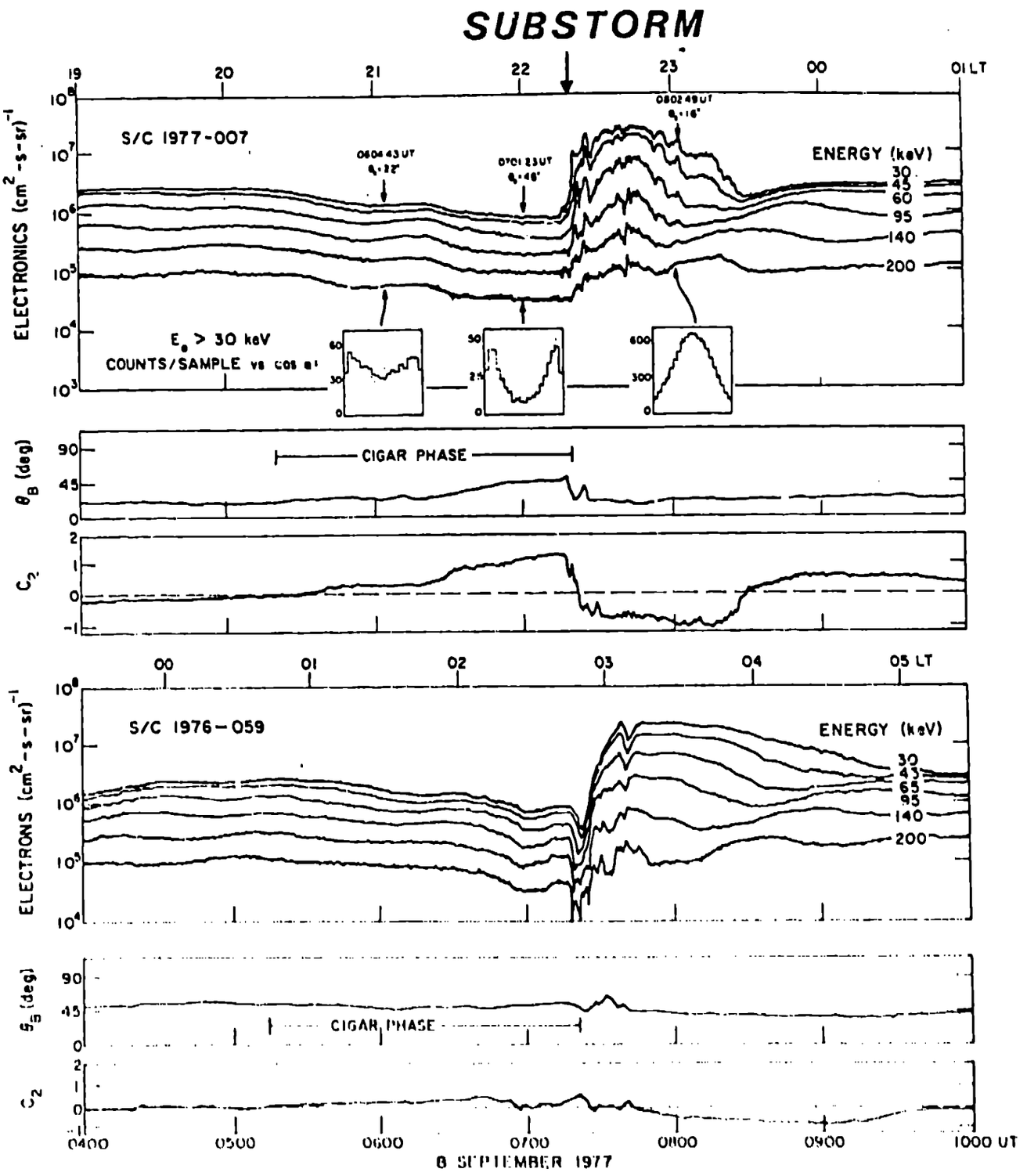
SUBSTORM
19
20
21
22
23
00
01 LT
S/C 1977-007
ENERGY (keV)
30
45
60
95
140
200
ELECTRONICS (cm²-s-sr)⁻¹
E₀ > 30 keV
COUNTS/SAMPLE vs cos α
θB (deg)
CIGAR PHASE
C2
00
01
02
03
04
05 LT
S/C 1976-059
ENERGY (keV)
30
45
65
95
140
200
ELECTRONS (cm²-s-sr)⁻¹
θB (deg)
CIGAR PHASE
C2
0400
0500
0600
0700
0800
0900
1000 UT
8 SEPTEMBER 1977

Fig 5

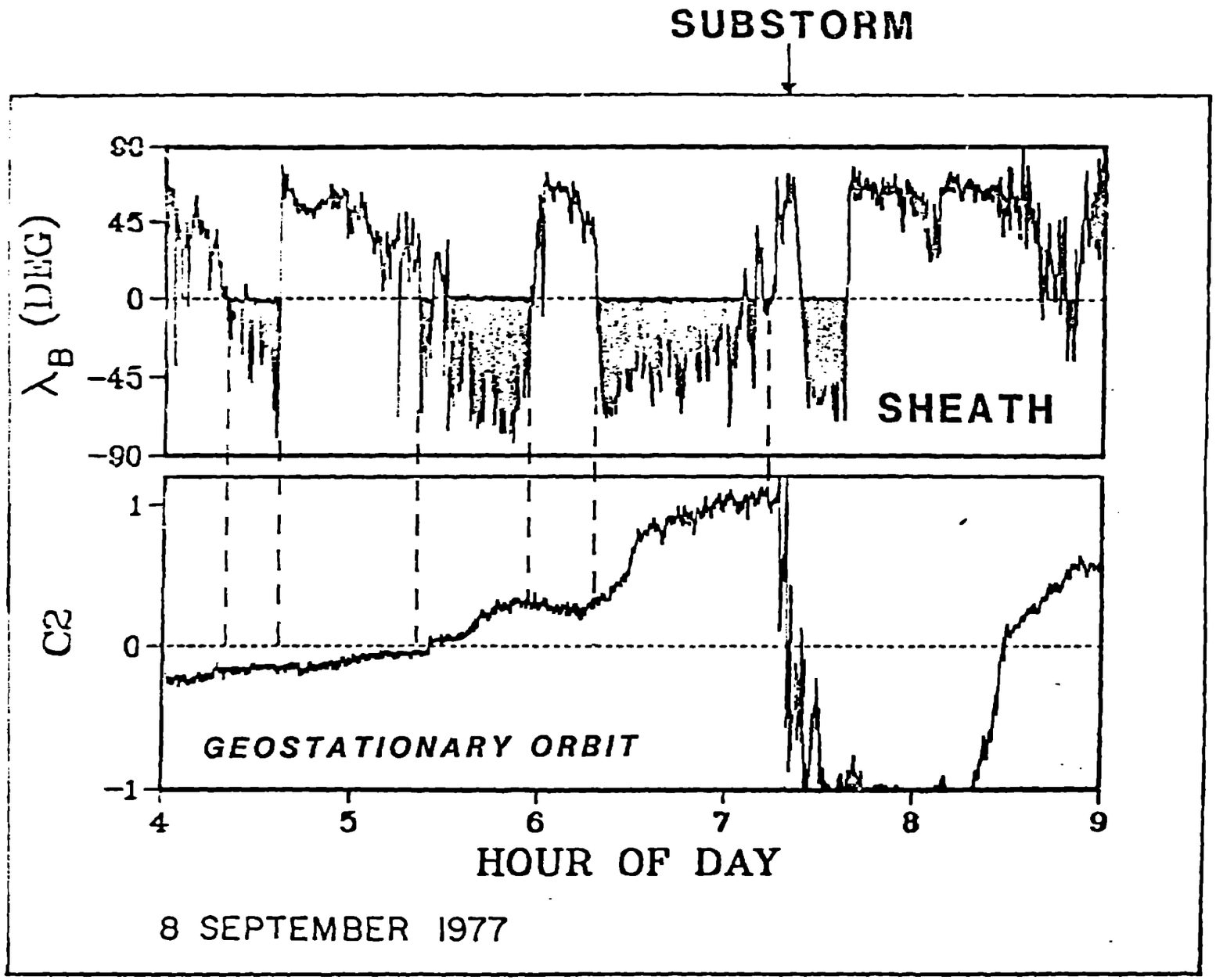
SUBSTORM
90
45
0
−45
−90
λ_B (DEG)
SHEATH
1
0
−1
C2
GEOSTATIONARY ORBIT
4
5
6
7
8
9
HOUR OF DAY
8 SEPTEMBER 1977

Fig. 6

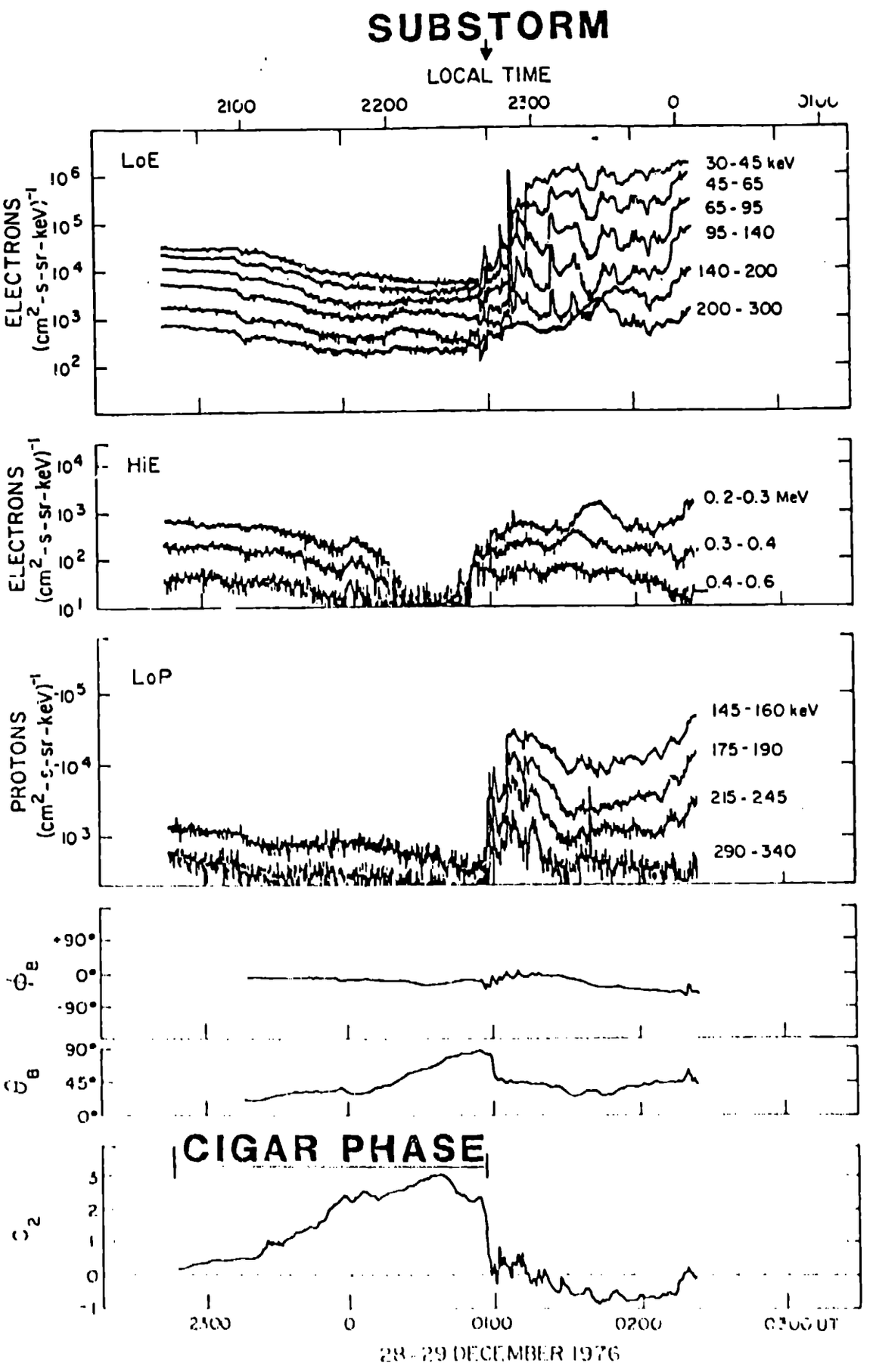
SUBSTORM
LOCAL TIME
2100
2200
2300
0
LoE
ELECTRONS (cm²-s-sr-keV)⁻¹
30-45 keV
45-65
65-95
95-140
140-200
200-300
HiE
0.2-0.3 MeV
0.3-0.4
0.4-0.6
LoP
PROTONS (cm²-s-sr-keV)⁻¹
145-160 keV
175-190
215-245
290-340
+90°
0°
-90°
90°
45°
0°
CIGAR PHASE
2300
0
0100
0200
UT
28-29 DECEMBER 1976

Fig 7

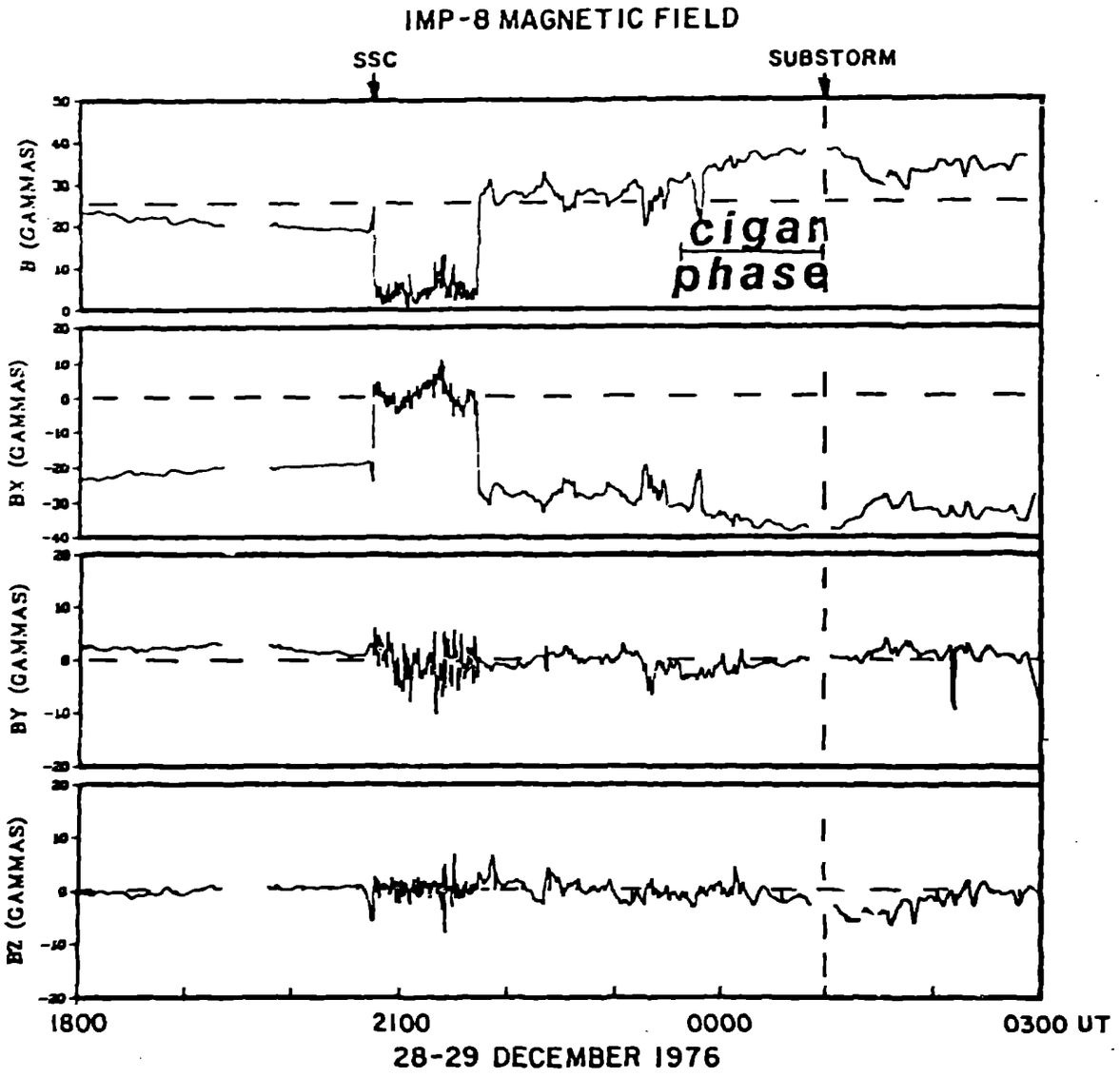
IMP-8 MAGNETIC FIELD
SSC
SUBSTORM
B (GAMMAS)
BX (GAMMAS)
BY (GAMMAS)
BZ (GAMMAS)
cigar
phase
1800
2100
0000
0300 UT
28-29 DECEMBER 1976

Fig. 8

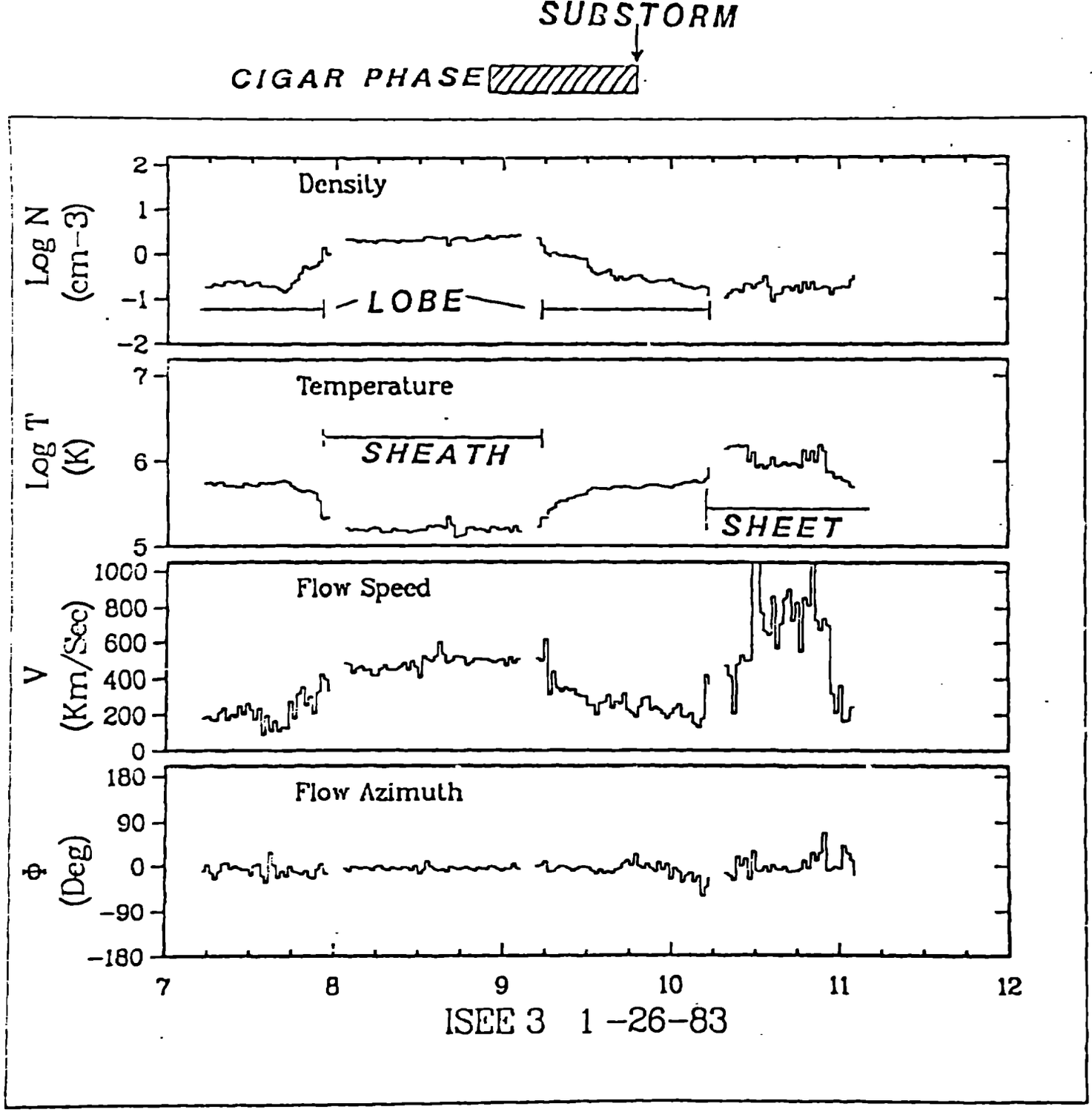
SUBSTORM
CIGAR PHASE
Density
Log N (cm-3)
2
1
0
-1
-2
LOBE
Temperature
Log T (K)
7
6
5
SHEATH
SHEET
Flow Speed
V (Km/Sec)
1000
800
600
400
200
0
Flow Azimuth
Φ (Deg)
180
90
0
-90
-180
7
8
9
10
11
12
ISEE 3 1-26-83

Fig. 4

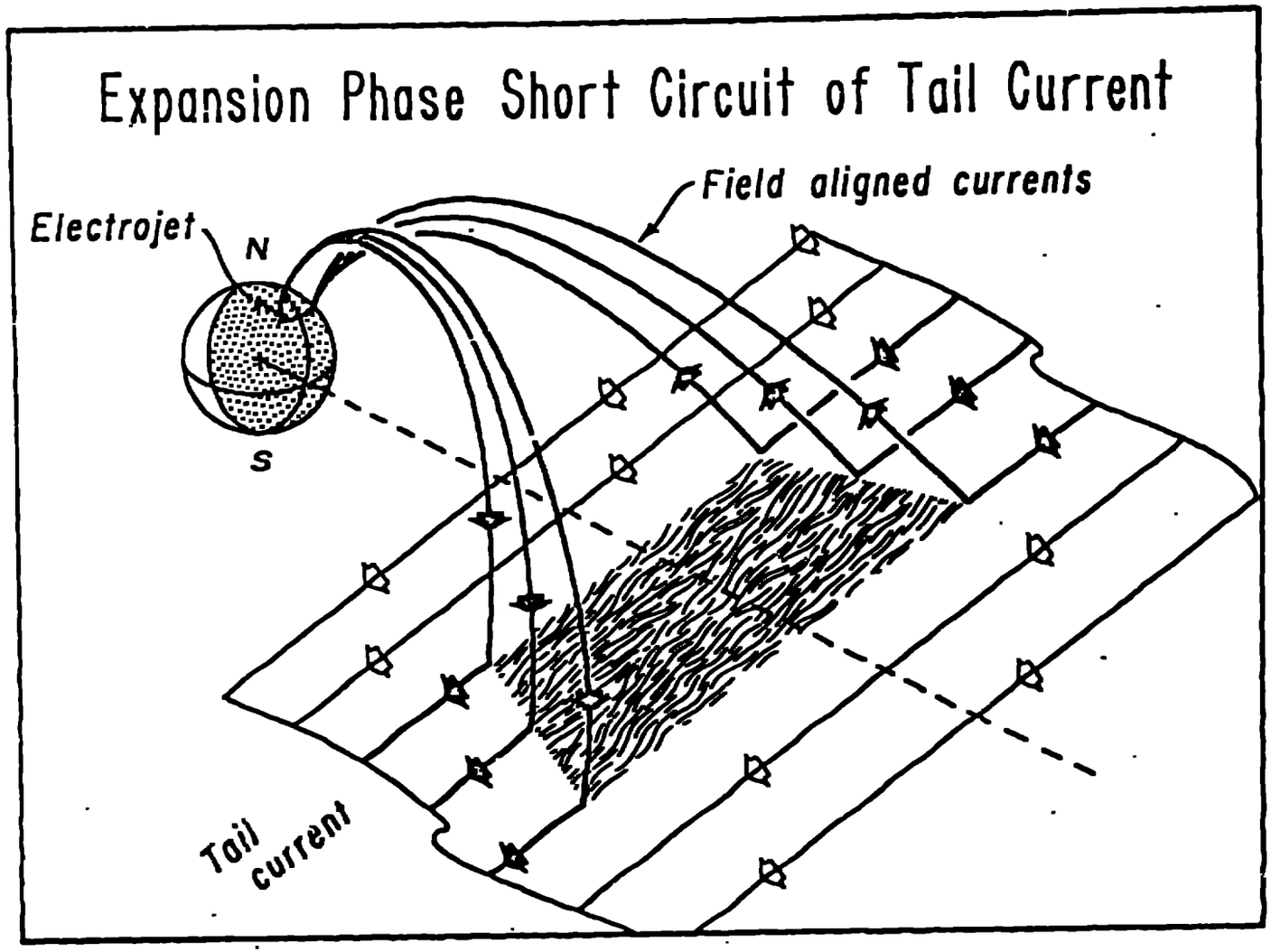
Expansion Phase Short Circuit of Tail Current
Field aligned currents
Electrojet
N
S
Tail current

Fig. 10

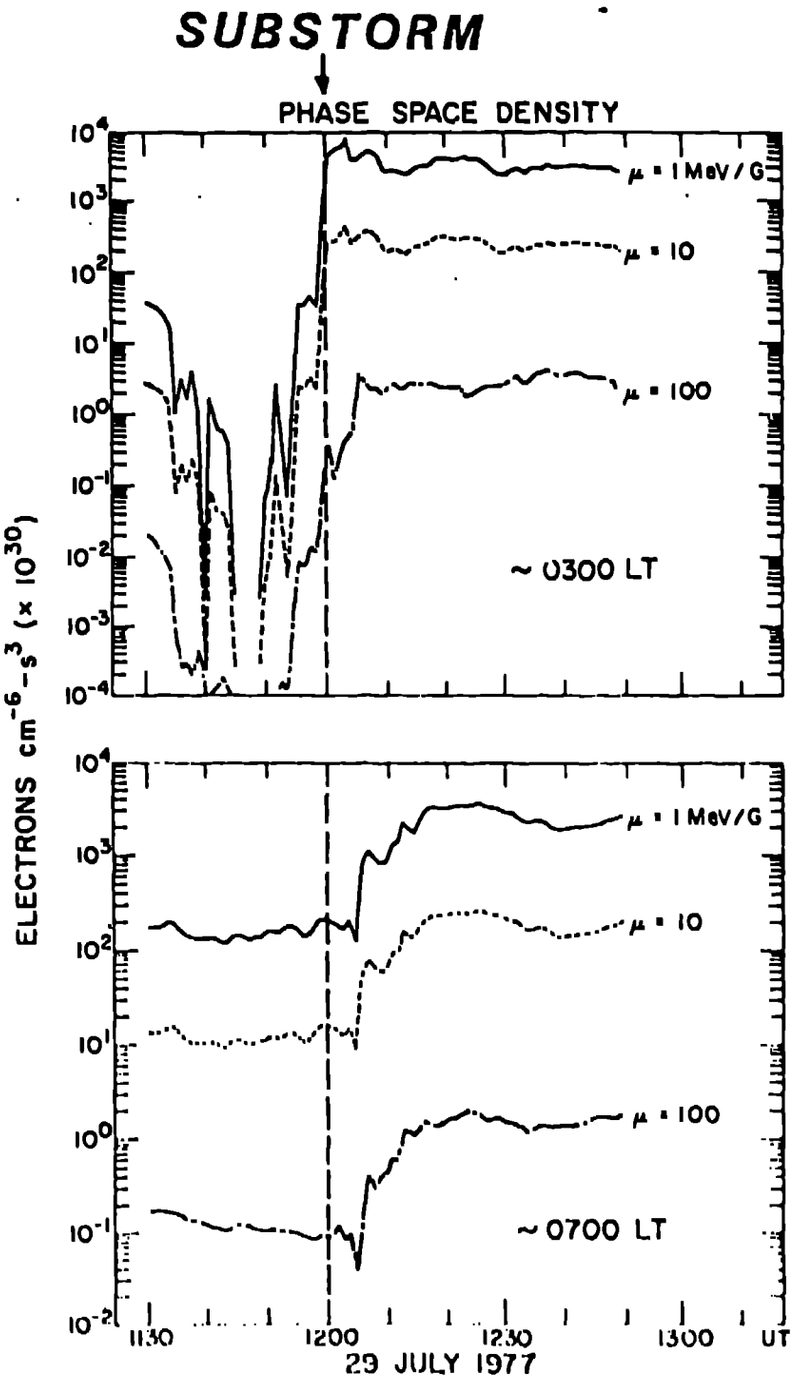
SUBSTORM
PHASE SPACE DENSITY
ELECTRONS cm^{-6}-s^3 (x 10^{30})
10^4
10^3
10^2
10^1
10^0
10^{-1}
10^{-2}
10^{-3}
10^{-4}
μ = 1 MeV/G
μ = 10
μ = 100
~ 0300 LT
~ 0700 LT
1130
1200
1230
1300
UT
29 JULY 1977

Fig. 11

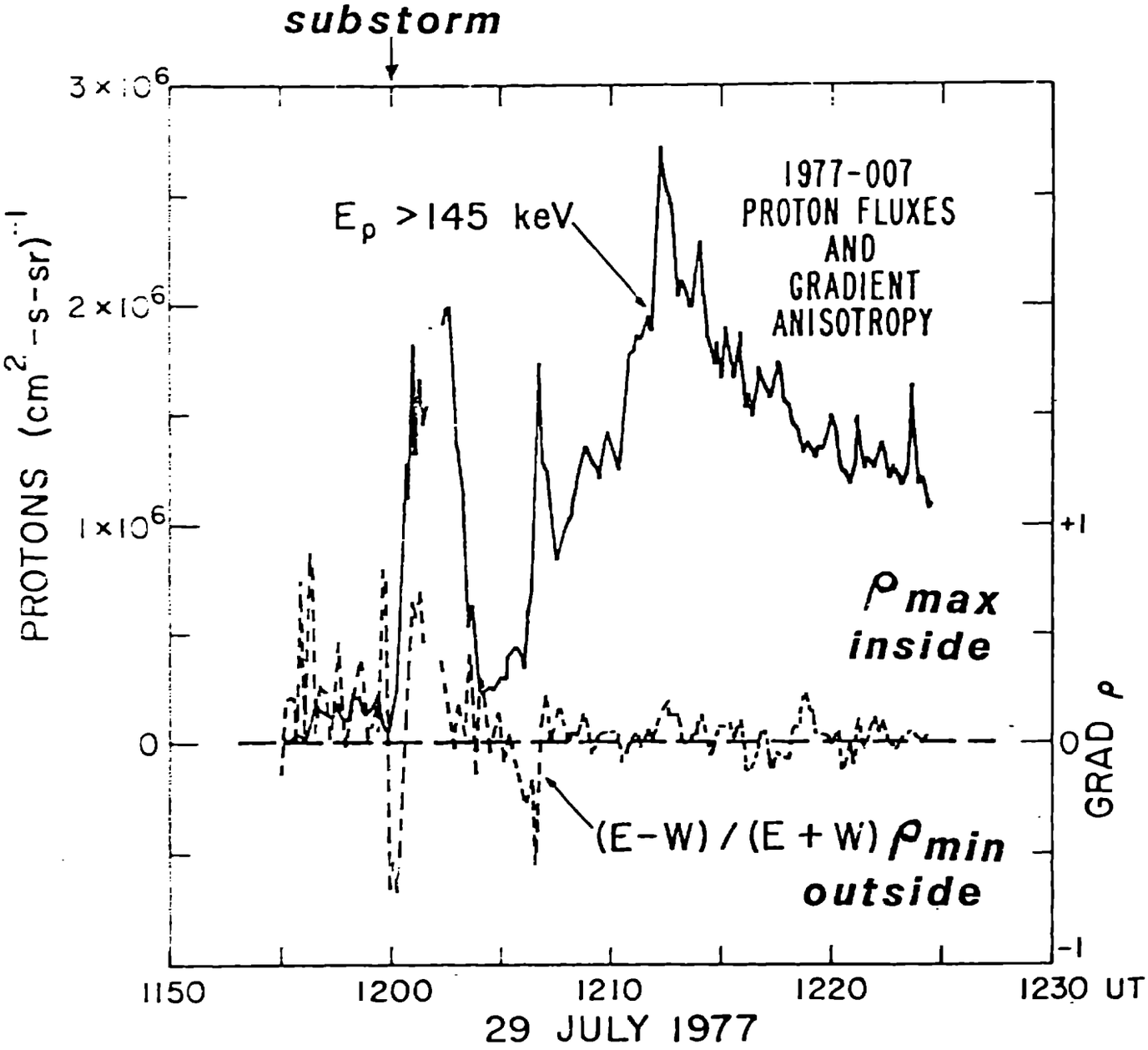
substorm
3 × 10^6
2 × 10^6
1 × 10^6
0
PROTONS (cm^2-s-sr)^-1
E_p >145 keV
1977-007
PROTON FLUXES
AND
GRADIENT
ANISOTROPY
ρ max
inside
(E-W) / (E + W) ρ min
outside
+1
0
-1
GRAD ρ
1150
1200
1210
1220
1230 UT
29 JULY 1977

Fig. 12

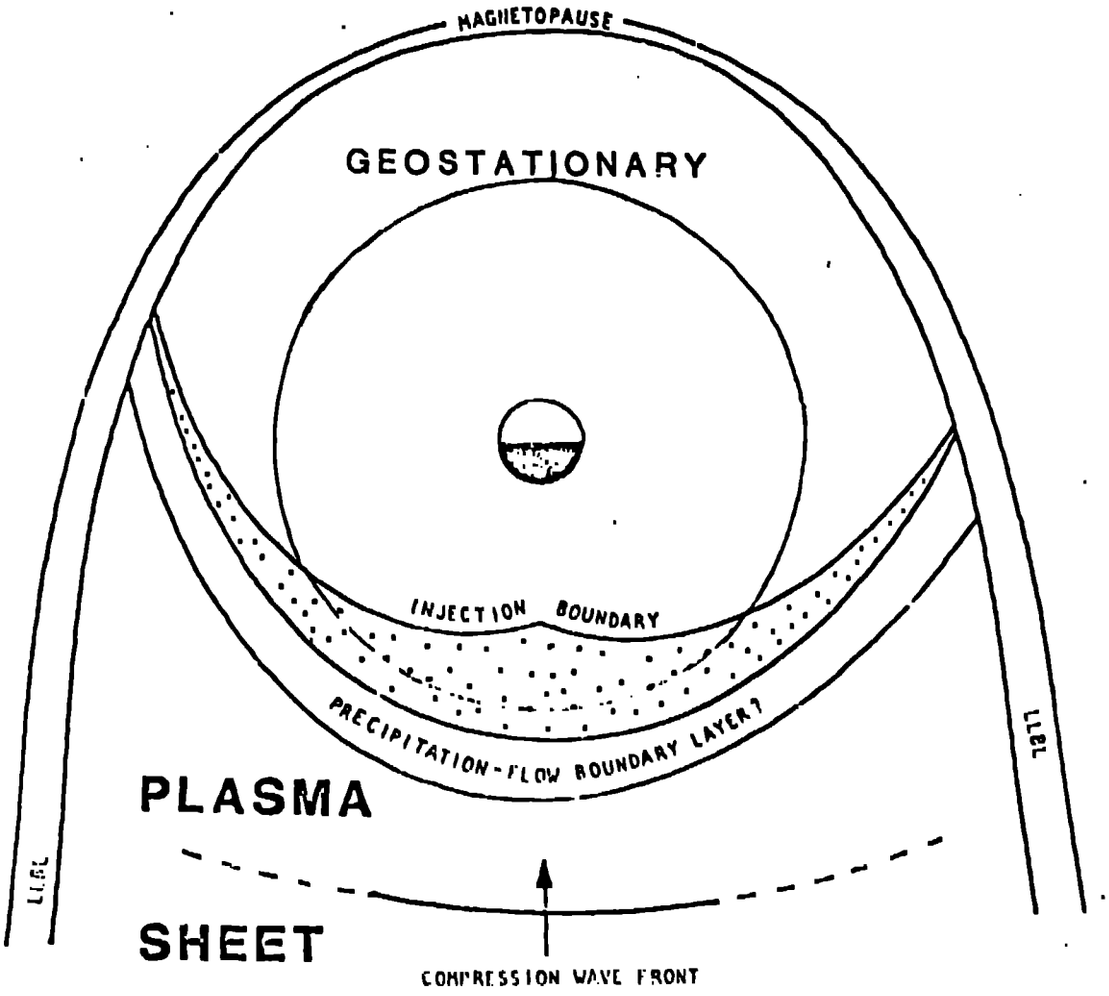
MAGNETOPAUSE
GEOSTATIONARY
INJECTION BOUNDARY
PRECIPITATION-FLOW BOUNDARY LAYER?
PLASMA
SHEET
COMPRESSION WAVE FRONT

Fig. 13

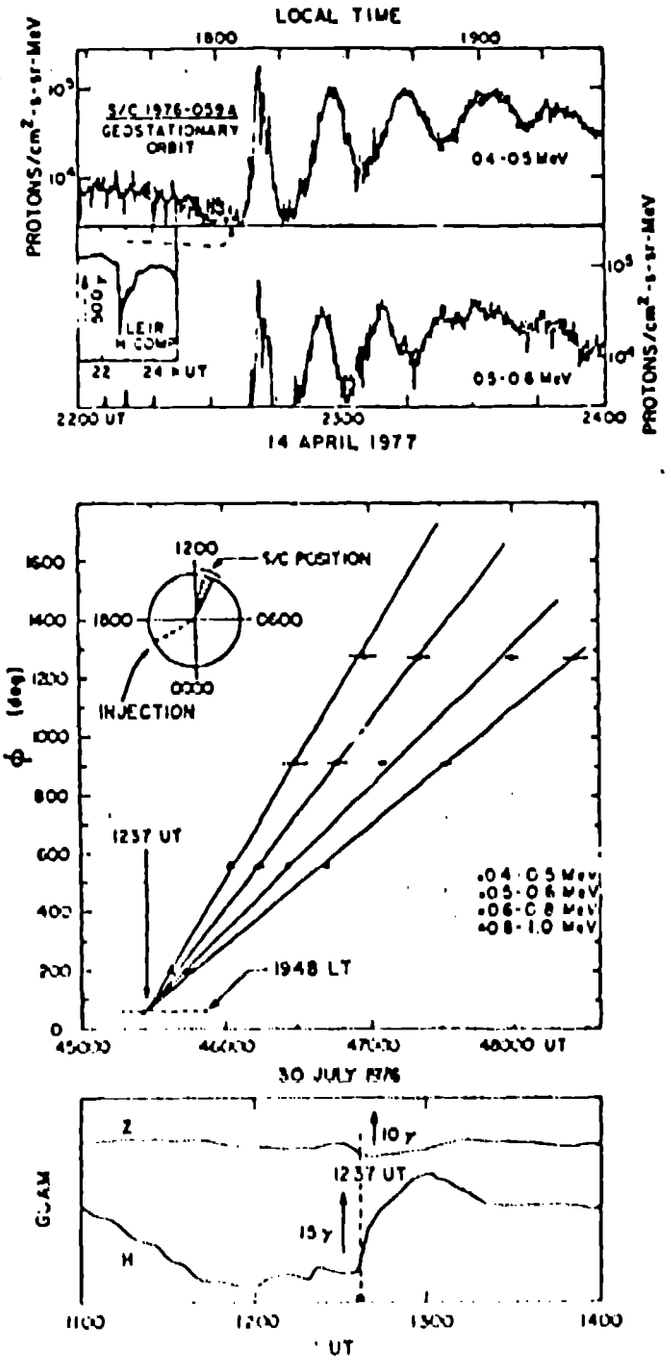
LOCAL TIME
1800
1900
PROTONS/cm²-s-sr-MeV
S/C 1976-059A
GEOSTATIONARY ORBIT
04-05 MeV
05-06 MeV
LEIR
H COMP
22
24 h UT
2200 UT
2300
2400
14 APRIL 1977
1200
S/C POSITION
1800
0600
0000
INJECTION
1237 UT
1948 LT
.04-0.5 MeV
.05-0.6 MeV
.06-0.8 MeV
.08-1.0 MeV
UT
30 JULY 1976
GOES
Z
10 γ
1237 UT
15 γ
H
1100
1200
1300
1400
UT

Fig 14

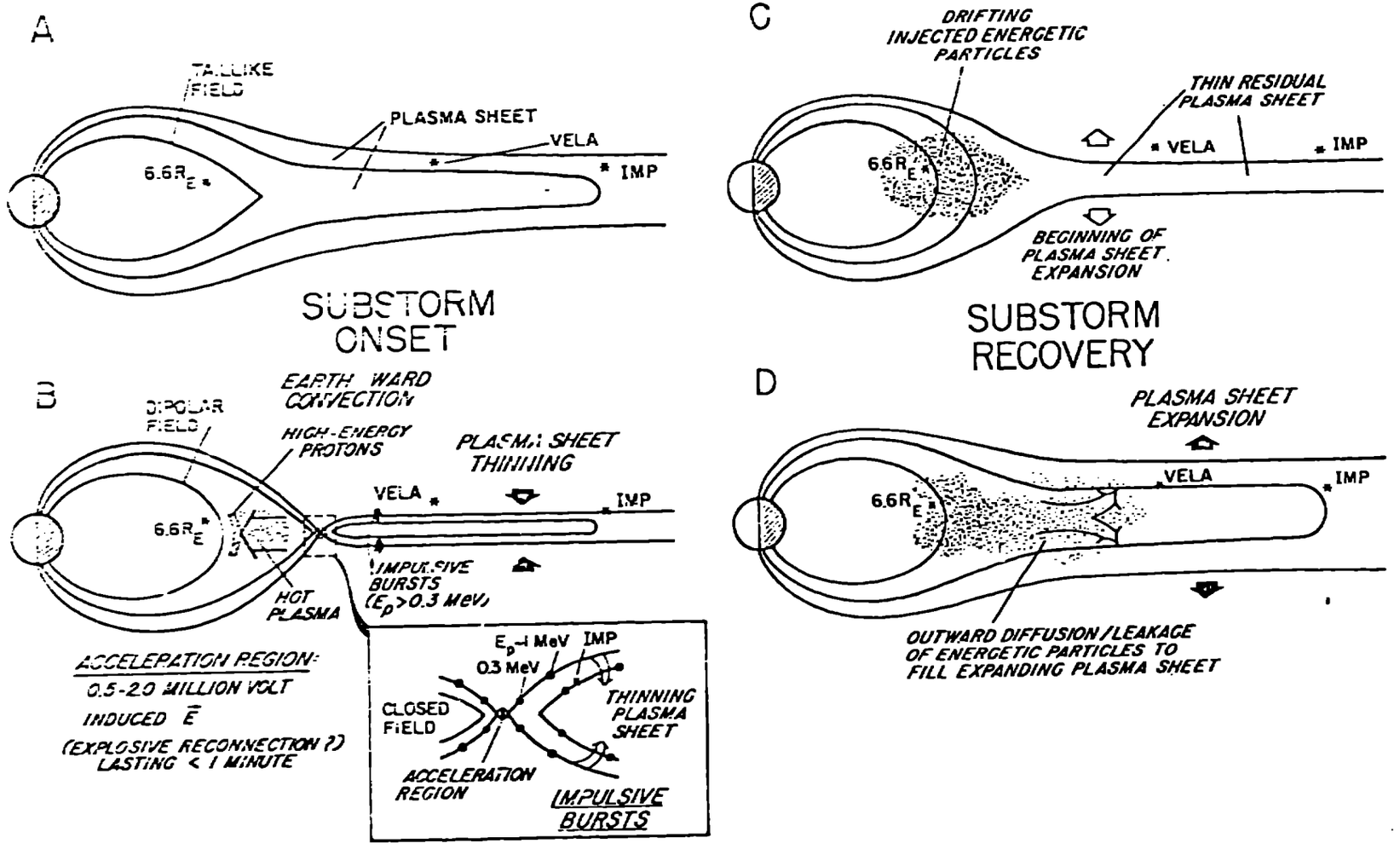
A
TAIL-LIKE FIELD
PLASMA SHEET
VELA
IMP
6.6R_E
SUBSTORM ONSET
B
DIPOLAR FIELD
EARTH WARD CONVECTION
HIGH-ENERGY PROTONS
PLASMA SHEET THINNING
VELA
IMP
6.6R_E
IMPULSIVE BURSTS (E_p>0.3 MeV)
HOT PLASMA
ACCELERATION REGION:
0.5-2.0 MILLION VOLT INDUCED E
(EXPLOSIVE RECONNECTION ?) LASTING < 1 MINUTE
E_p~1 MeV
0.3 MeV
IMP
CLOSED FIELD
THINNING PLASMA SHEET
ACCELERATION REGION
IMPULSIVE BURSTS
C
DRIFTING INJECTED ENERGETIC PARTICLES
THIN RESIDUAL PLASMA SHEET
VELA
IMP
6.6R_E
BEGINNING OF PLASMA SHEET EXPANSION
SUBSTORM RECOVERY
D
PLASMA SHEET EXPANSION
VELA
IMP
6.6R_E
OUTWARD DIFFUSION / LEAKAGE OF ENERGETIC PARTICLES TO FILL EXPANDING PLASMA SHEET

Fig. 15

SCATHA

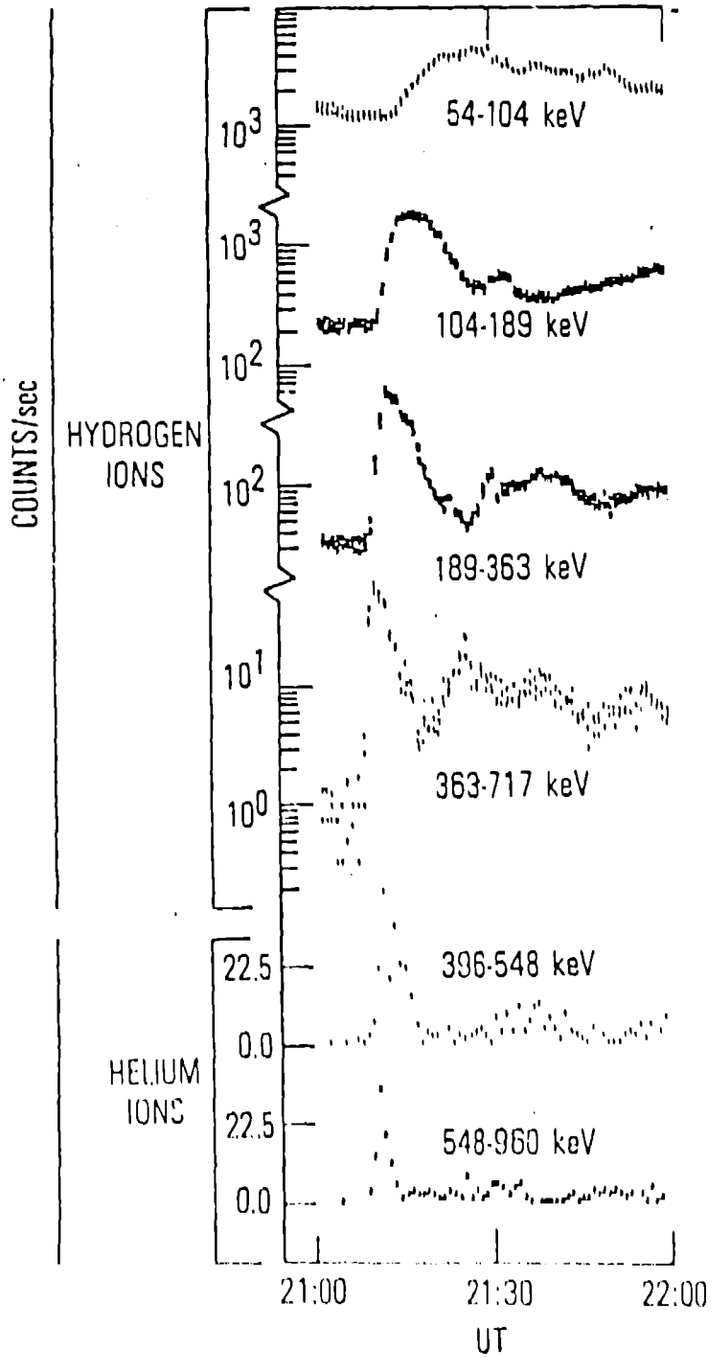

FEBRUARY 25, 1979

Fig. 16